Regression Analysis of Wetting Characteristics for Different Random Surface Roughness of Polydimethylsiloxane Using Sandpapers

Moutushi Dutta Choudhury[1], Saptarshi Das[2, 3], Arun G. Banpurkar[4]and Amruta Kulkarni[4]

1) *Department of Physics, Chandigarh University, NH-95, Ludhiana - Chandigarh State Hwy, Punjab140413, India (Email: moutushi.e9474@cumail.in,mou15july@gmail.com)*
2) *Department of Mathematics, College of Engineering, Mathematics and Physical Sciences, University of Exeter, Penryn Campus, Penryn TR10 9FE, United Kingdom. (Email: saptarshi.das@ieee.org, s.das3@exeter.ac.uk)*
3) *Institute for Data Science and Artificial Intelligence, University of Exeter, North Park Road, Exeter, Devon EX4 4QE, United Kingdom.*
4) *Department of Physics, Savitribai Phule Pune University, Pune, 411007, India. (Email: agb@physics.unipune.ac.in, amrutakulkarni611@gmail.com)*

Abstract

This paper studies various wetting characteristics on different surfaces of Polydimethylsiloxane (PDMS) polymer. The random roughness of the surface is engineered by using sandpapers to introduce different order of hydrophobic properties to understand the temporal evolution of drying droplets. We develop statistical models to predict temporal evolution of the base diameter, height, surface, and contact angle of drying droplets with varying grit size or surface roughness. Five different robust polynomial regression models have been compared for the prediction of three dependent variables - base diameter, height, and surface of drying droplets for random rough surfaces. In a nutshell, we here identify the best statistical model to capture the dynamics of drying droplets on hydrophobic surfaces of random roughness characteristics.

Keywords: robust polynomial regression; wetting; contact angle; droplet characterization; random rough surface; statistical modelling

1. Introduction

The pattern formation on solid surface, from micrometer to nanometer size, is commonly engraved for fundamental studies of surface property. Wetting of liquids on rough and patterned surfaces is used in many technological and medical applications such as micro or nano-fluidics, microelectronic devices, video display, integrated circuits, electronic chip etc. [1], [2]. There are numerous patterned surfaces found in nature and they have special significance, e.g. the self-cleaning property of leaf surface is possible due to the hierarchy of micro to nano structures [3]. Butterfly and bird feathers have structural colors and fine hairy structures [4], [5]. Reptile like Gecko's feet has good adhesion properties due to nano-structures [6].

The study of "anti-wetting" and "super-wetting" properties of surfaces have high demand in the field of surface-interface research and most of the studies are done on considering either Cassie-Baxter or Wenzel model [7], [8]. Both these traditional models consider the periodic structures. Nature is full of examples of natural periodic structured surfaces [9] which can be distinguishably observed using above mentioned two wetting models. But randomness or disorder is another natural phenomenon which also introduces super-hydrophobicity and superoleophobicity as found in many natural surfaces. Quantifying surface complexity is another big challenge for the current research needs for reproducibility and predictability of surface properties. During free evaporation, or phase transition of the liquids from the surfaces change the solid-liquid sites to liquid-vapor sites, and there could be stages which involves Cassie-Baxter to Wenzel transition. Experimentally these transitions are difficult to quantify. Water can be trapped inside the pores and during the drying process. Capillary force gravitational force and adhesive

forces between the liquid and the surface molecules etc. forces could also be considered. These involves phenomenology with molecular dynamics simulations, which is studied in recent works like [10]. Now, apart from involving the details of the complexity, which is difficult to realize in established theories, droplet dynamics features directly extracted from experimental data can also suggest us about the drying properties or the de-wetting property of the surface. Drop base diameter or height changing or surface area changing with time basically implies here dynamical change in the drop features. Therefore, instead of looking at the molecular level of surface – liquid interaction, someone can look only at the above-mentioned parameters of a drop and correlation analysis can give us information about what type of drying. Since constant contact angle (CCA) or constant contact radius (CCR) are mainly two methods of drop-dynamics change, some absorptions or adsorptions can take place during drying on random surface which can also be quantified by different drop-drying dynamics models. It is independent of the molecular interactions which is not investigated in this study.

1.1 Relevant Previous Works

Now a days, in many real-world engineering and biomedical applications, metals are replaced by polymers due to their extraordinary properties like light weight, compatibility, durability, cost effectiveness and availability. Several non-conventional methods like self-assembly mono layer (SAM), colloidal assembly and template guided pattern formation are commonly used to engineer different types of surfaces [11].

Surface quantifications in the vicinity of its wetting properties has been done since last seven decades. Cassie-Baxter model for rough surfaces with air trapping between the surface and the drop has been studied thoroughly because of its vast applications in the field of painting industry to the oil recovery industry. Study of roughness of the polymeric surfaces and nano composite surfaces is one of the huge areas of interdisciplinary research because of modern age hydrophobic surface-product demands from everyday engineering applications to the biomedical applications. In recent time, polymer surfaces are modified by different researchers worldwide. Daily use substrates, like Polystyrene, could be modified by using plasma treatment [12]. Roughness is introduced by activating the surface polymers and depositing the functional group to the surfaces. Similarly, the opposite can also be done by introducing wetting enhancing group on the surfaces [13]. Another surface modification can be achieved by depositing nanocrystalline structures to the surfaces using different coating methods to modify hydrophobicity and wetting properties [14].

After detection of the COVID-19 virus properties in the last two year, researchers are also curious about finding its drop adhesion on different kind of substrates, simple glass substrates to different polymeric substrates [15], [16]. For instance, Sarkar *et al.* worked on the dynamic contact angles measurement on rough surfaces by sessile-droplet and captive-bubble methods [17]. This study tracked the regimes of applicability of the above-mentioned methods experimentally and theoretically using sandpaper induced metal rough surfaces. Researchers have also proposed engineered antiviral surfaces to stop the spread of COVID-19 virus [18]. Cold spray copper coating was also used to reduce the lifetime of COVID-19 virus as compared to the stainless steel used as the push plates of publicly accessed buildings and hospitals [19].

Polydimethylsiloxane or PDMS is a polymer that has drawn huge attention of interdisciplinary surface science field because of its unique wettability characteristics, surface stability and ability of flawless mimicry of surface characteristics [20], [21]. Amongst different wettability characteristics, the super-hydrophobicity is one of the most desired properties for self-cleaning surfaces. PDMS is a highly non-conducting substrate and poor conductor of heat [22]. Also, composites of PDMS e.g. Zinc Oxide (ZnO)/PDMS combination and poly[hexeafluorobisphenol A-co-cyclotriphosphazene] microspheres (PHC)/PDMS or PHC-PDMS combination increase anti-icing property of the surface [23], [24]. Self-recovering property after the application of high stress and super-hydrophobic process stability of PDMS

composite surfaces, make them more desirable for aircrafts and power lines [24].

PDMS is also used to form microfluidic devices by using its ability of replicating different surfaces by soft lithography techniques [2]. Also, it changes its wettability very easily when it goes through oxygen plasma treatment [25]. The surface of the PDMS is changed due to the introduction of hydroxyl groups. PDMS helps some bio-proteins e.g. Zein film, consisting of both hydrophilic and hydrophobic amino-acids to replicate three dimensional patterns and change its wettability properties with desired masks [25]. Acetobacter xylinum, an aerobic bacterium, synthesizes bacterial cellulose (BC) preferably on the ridge surfaces of PDMS. It can be well observed by polarizing microscope because BC fibrils develop uniaxially oriented liquid-crystal like domain, only when they grow on a certain ridge sized PDMS surfaces.

Biomimicry is one of the recognized procedures to study various skins of living systems. Self-healing and biomimetic properties of PDMS make it suitable for many bioengineering applications [27]. Also, PDMS is tribo-electrically less positive than human skin, very flexible which makes it suitable for higher degree of charge transfer from human skin to PDMS structured surfaces and to construct low cost polymer based triboelectric energy harvesting pedometer [28].

Structured PDMS is a widely used polymer to make triboelectric nanogenerators (TENG) [29], [30]. Increased effective contact area also increases induced surface charge density by tribo-electrification process. The variations of the ranges of grit numbers of sandpapers are quite inexpensive and easily available in the market. Pattern formation on PDMS can be done by using these sandpapers using the accurate replication property of PDMS. This kind of surfaces along with different metal electrodes make them effective for applications like TENG [29], [30].

1.2 Methodological Novelty of This Paper

Self-cleaning or ice-phobic surface is achieved by increasing hydrophobicity of the surface by introducing micro-nano structures on the surfaces by growing periodic micro-nano pillars which are the recent trend of research, especially in the study of wettability [31], heat transfer in condensation [32], super-hydrophobicity and water repellency [33], super-hydrophobicity using plasma polymerization [34] and silica nanoparticles [35]. Controlling periodic constant height pillars on surfaces or the deposition of another material to grow nano-pillars and stabilizing them on the surfaces could be more difficult to control, costly and time-consuming process. Moreover, growth of the condensed droplet, rolling-slipping of the drop or impact of the drop on nano-pillar embedded-surface is quite a laborious exercise to realize and to get stabilization of the surface roughness [33]–[35].

Sessile drop technique of measurement of surface tension is used to characterize a solid surface energy by using a droplet of known surface tension [36]. The shape of the drop changes with the surface energy, in other words, by the structure of the surface. The observed parameter here is the contact angle and its different versions like static, dynamic, advancing, receding or retreating contact angles [36]. We have used the Goniometer for measuring contact angles as described in [37].

In this study, we have extended common characterization of surface wettability of PDMS structured surfaces. Our study is mainly related to imitate random structure, their morphology and surface roughness. The polymer PDMS solution is commercially available thus it is easy to prepare the film on the sandpapers by using the soft lithography method [38]. PDMS is a chemically inert polymer which is important criteria for an ideal substrate. It is easy to manufacture the microstructures or replica of sandpaper on PDMS surfaces. However, the study of random surface morphology is lacking in the previous literature, which is the main focus of this paper. Surface morphology or roughness is usually characterized by contact angle goniometer measurements. Our goal here is to study the effect of surface roughness on the equilibrium and temporal dynamics of wetting behaviors.

As highlighted above, there are very few previous works which have studied the effect of grit size especially hydrophilic and hydrophobic behavior on temporal evolution of drying droplets on PDMS surfaces. We initially estimate the surface roughness probability density function from confocal images for varying grit size to characterize the surfaces. We study temporal evolution of key droplet drying parameters e.g. base diameter (BD), contact angle (CA) – left (LCA), right (RCA) and mean (MCA), height (*H*), surface (*S*), volume (*V*) and their changes with different surface roughness or grit size (GS). The small variation amongst multiple repeated trials (5-10 repeats) of the experiments on the same surface are characterized using statistical methods like multivariate distribution or pair-plots and robust polynomial regression analyses. The correlation analysis amongst these variables will allow us to understand the linear vs. nonlinear relationships between these attributes of the droplet and can be useful for studying similar droplet drying characteristics in other similar systems as well. Therefore, the main aim here is to show how the contact angle varies as a linear or nonlinear function of the specified grit size or surface roughness and also establishing empirical statistical models using repeated experimental data.

There have been few analytical studies on droplet evaporation kinetics mostly on isolated and suspended droplets without any surface interactions [39] and on hydrophilic smooth substrates [40]. However, our study primarily addresses similar effects on hydrophobic surfaces which are difficult to analyze using analytical solutions such as spherical or ellipsoidal cap formula, particularly on random structured surfaces which can be approximated by an underlying probability distribution of the grains or ridges embedded on the surface. There have been very few analytical treatments of droplet evaporation kinetic modeling for strongly hydrophobic [41] and superhydrophobic surfaces [42], which cannot be easily extended to random structured rough surfaces. Moreover, due to the difference in volume of the droplets, a generalized mathematical modelling treatment of droplet evaporation kinetics will not be able to capture these nonlinear and stochastic behaviors due to different size of the drops which can only be captured through repeated experiments. This motivates us to develop a robust statistical model through robust polynomial regression analysis as compared to the analytical solutions of the underlying complex governing physical laws which typically involves many approximations of the properties of the surface-fluid interactions.

2. Materials and Methods

2.1 Materials

The polymer polydimethylsiloxane (PDMS) (SYLGARD, Germany) 184 has been used to form polymer surfaces. It consists of silicone elastomer and curing agent. The Polystyrene Petri-dishes are used to pour the polymer during aging. These are cleaned by Laboline solution (Fisher Scientific) and dry them with the help of nitrogen blow. Random roughness on the surfaces is introduced by sandpapers (abrasive waterproof paper by John Oakey, India) of different grit size -220, 320, 400, 600, 800, 1000, 1500 and 2000. They are cleaned by nitrogen air jet pump for removing any impurities on it. Double distilled water and micropipette (Thermo scientific – fine pipette F3) has been used for measuring wettability.

2.2 Methods

To prepare random rough surfaces, PDMS is prepared as a mixture of silicone elastomer and cross-linker in the ratio of 10:1 by weight. The mixture is stirred for 15 minutes to mix it well and then degassed it for 30 minutes to remove all the air bubbles from the solution. Then, we take the sandpapers of different grit sizes ranging from 220 to 2000 and then cut them into small pieces of size 2cm×2cm. Larger the number of grit size makes the sandpaper finer. The sandpapers were cleaned by nitrogen jet to remove any impurities. Then the papers are stacked to the petri-dishes with the help of adhesive double-sided tapes. The PDMS solution is poured on the sandpapers. During pouring, precautions should be taken to avoid formation of air bubbles in the samples. Then annealing of the samples has been done in oven at 70°C for 24 hours. After reaching the room temperature the sample becomes transparent and

looks like a thin elastic membrane. Then we peel off the sandpapers from PDMS. Nitrogen air jet is blown through the samples for getting them sand-free. The film thickness is maintained to be ~2 mm.

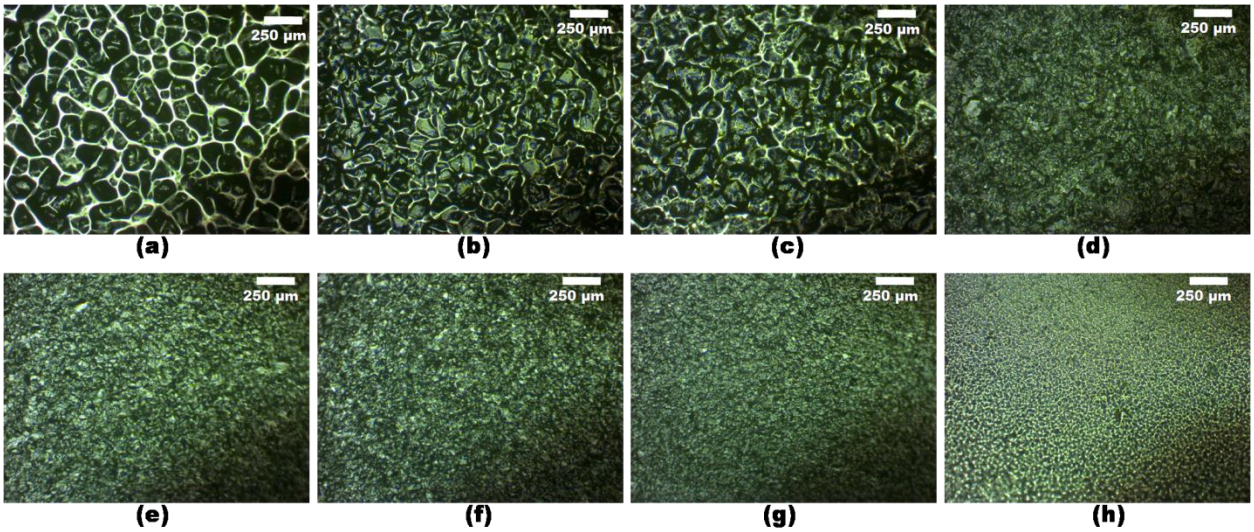

Figure 1: Microscopic images of random rough substrates, taken by confocal microscope. (a)-(h) for varying grit size of 220, 320, 400, 600, 800, 1000, 1500, 2000 respectively. The scale is in μm.

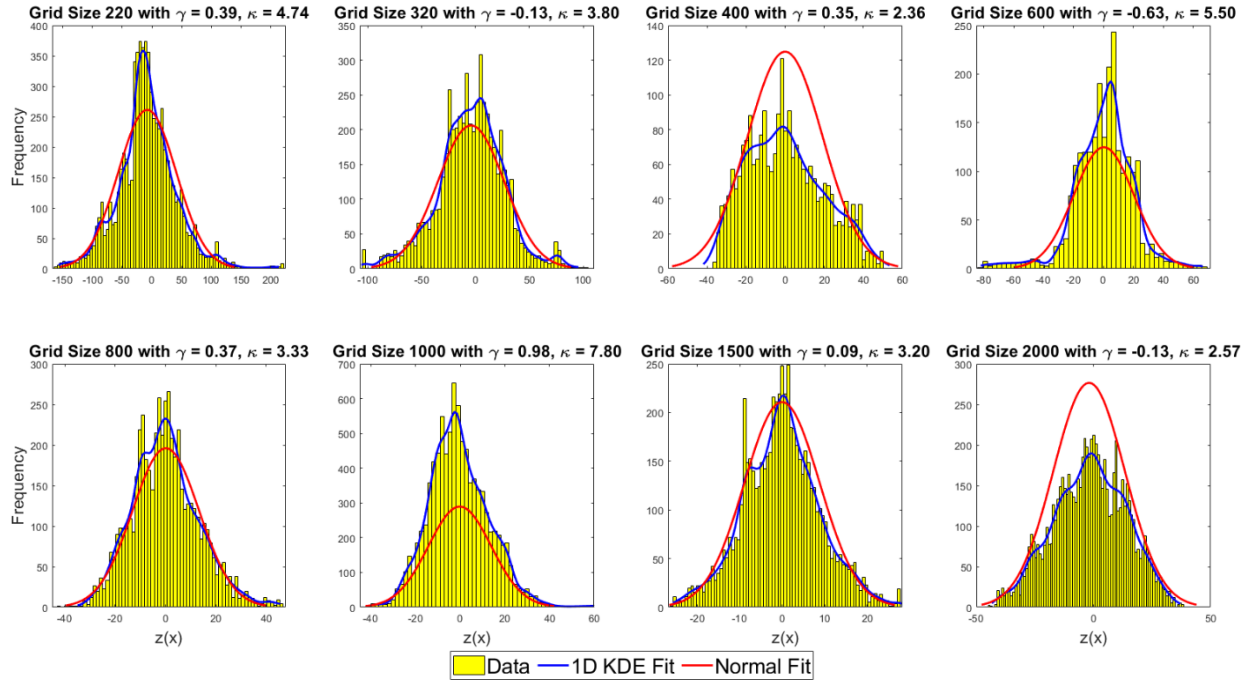

Figure 2: Roughness analysis for grit sizes: (a) 220, (b) 320, (c) 400, (d) 600, (e) 800, (f) 1000, (g) 1500 and (h) 2000. Here, $p(z)$=normalized frequency of the probability density function, $z(x)$=roughness profile in μm.

Figure 1 shows the confocal microscope images of 8 different grit sizes and the corresponding roughness plots are shown in Figure 2. The roughness was measured at different positions of the surface and then reshaped as a single 1D data vector for the statistical analysis. It is evident from the discrepancy between the 1D kernel density estimate (KDE) of the roughness histogram and the equivalent normal

distribution fit with the sample mean and standard deviation that the simple normal fit has mostly underestimated the density except grit size 400 and 2000 where we observe an overestimated histogram. The sample skewness (γ) and kurtosis (κ) parameters indicate that except grit size 1500, almost all of them significantly differ from the equivalent normal distribution with sample mean and standard deviation. Highly leptokurtic or super-Gaussian distributions are observed for the surface roughness data with grit size 600 and 1000. The corresponding normal probability plots in Figure 3 affirms this finding while comparing the fitted distribution with respect to an equivalent normal distribution which clearly deviates due to the fat tails of most surface roughness distributions. This non-Gaussian behavior of surface roughness has also been reported in [43] for minimum friction/stiction and using color distribution statistical matrix in [44].

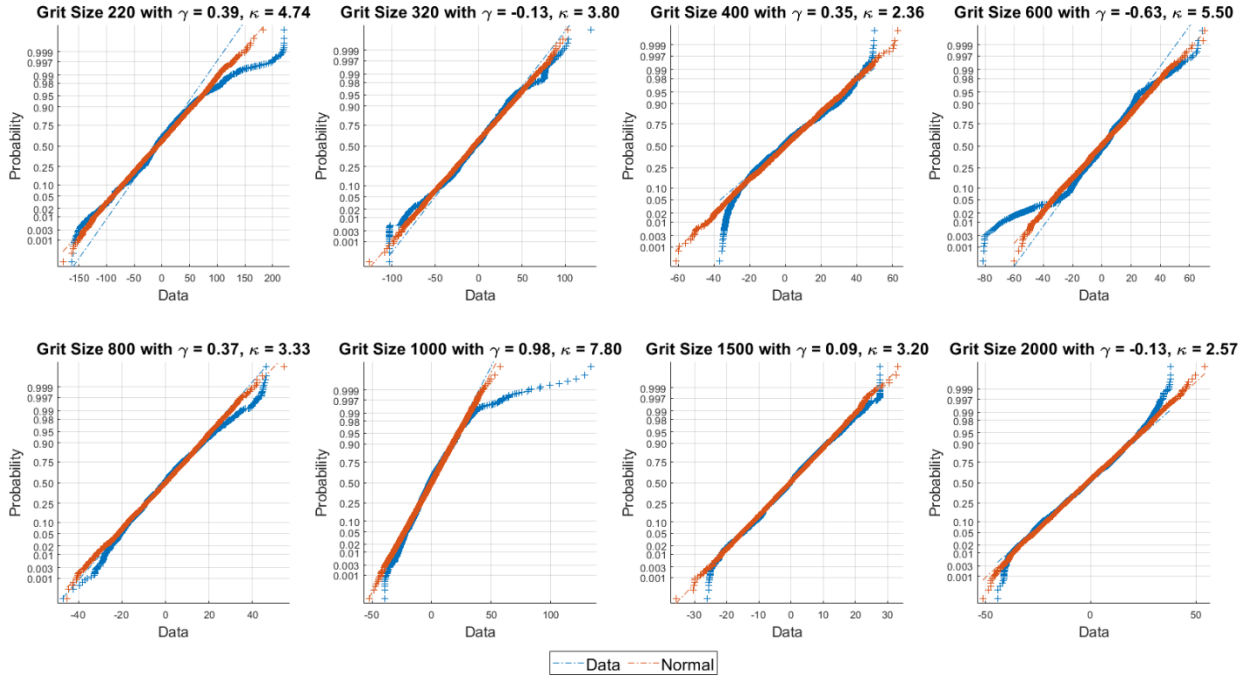

Figure 3: Normal probability plot of the surface roughness data for grit sizes: (a) 220, (b) 320, (c) 400, (d) 600, (e) 800, (f) 1000, (g) 1500 and (h) 2000, along with the respective skewness (γ) and kurtosis (κ) values.

To observe the microscopic structures of the surfaces, we use optical microscope (AxioVert Zeiss-135). The structures of surfaces are well studied through different magnifications. The Leica DCM 3D dual core measuring microscope is used to capture the images and it is analyzed by the software (Leica DCM 3D 3.3.1) [45]. It can stack the height (amplitude) parameter of given rough surfaces and analyze the roughness of the samples having thickness of 2 mm. Wetting behaviors are observed by placing water droplets of ~5μl on different rough substrates. The relative humidity (RH) condition of the room was recorded as 45% and ambient temperature was maintained at 25ºC. Wettability of the surfaces are measured by optimal contact angle (OCA) Goniometer and the data is analyzed using SCA 20 (Data Physics Instruments, GmbH) software [46]. Time evolution of contact angle, base diameter, height, and volume of drops are estimated by automated optical contact angle of sessile drop method. All instruments were referenced.

In Figure 1 some porosities can also be observed on the rough surfaces. It is well known that water molecules cannot be adsorbed in PDMS polymer. Since various proportion of the water droplet may get confined in the holes of irregular grit shapes even for the same grit size, it will affect the size and shape of the droplets in each experiment. These phenomena are difficult to model from first principle due to the

randomness of the surface which sets the ground for using experimental data-driven statistical modelling techniques instead.

In our study, the grit size is known beforehand since it is a specified quantity for the surface and takes discrete values which are not directly measured in our experiments. Grit size and the roughness in Figure 4 are related quantities and are inversely proportional to each other but the former is not directly measured. For a fixed grit size, the roughness pattern can vary because of the irregular microstructures of the grit. Using the measured roughness in the statistical model would have made it even more difficult to predict the outcomes as compared to the fixed specified variables like the grit size. Figure 4 shows that for fixed grit size, we are experimenting on a random surface, but the measure of randomness is not meant to be used in the modelling exercise for the droplet drying. For the same grit size and surface, depending on the location of the measurement, the surface roughness may vary which are shown using the mean ± one standard deviation ($\mu \pm \sigma$) of each of the 8 experimental cases in Figure 4.

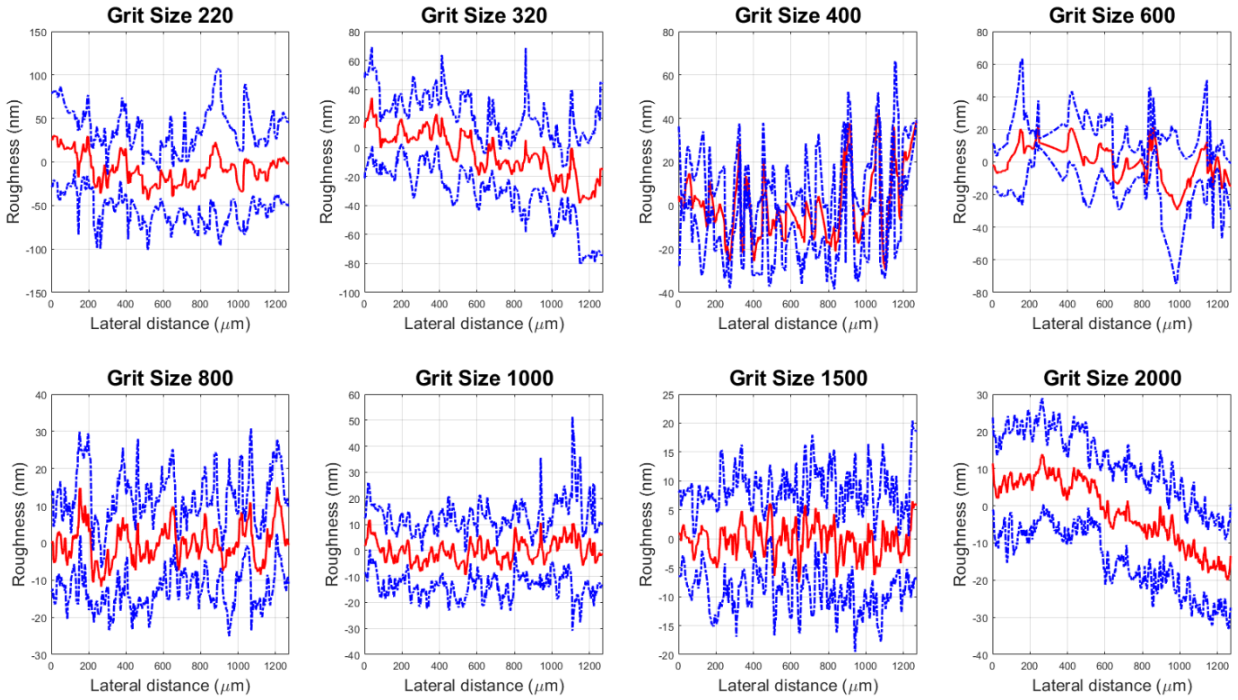

Figure 4: Variation of surface roughness as a function of lateral distance for different grit size. The measurements were taken at multiple places of the surface. The scale is in μm.

3. Imaging Results

Surfaces of different grit size are characterized by confocal images on which different measurements were taken for droplet evaporation with interaction with the substrates i.e. contact angle, evaporation and most importantly the surface morphology.

3.1 Confocal Image

Surface morphology of the substrates is observed with the help of optical confocal microscope. Figure 1 shows the confocal microscopic images of the rough substrates of PDMS with different grit sizes -220, 320, 400, 600, 800, 1000,1500 and 2000. We have used these images to find the approximated roughness of the substrate using Leica DCM 3D 3.3.1 [45]. In the following sections, statistical analyses of the roughness of the substrates have been illustrated.

3.2 Roughness Analysis from Confocal Images

The infrared confocal microscopy Leica DCM 3D [45] load up the height (amplitude) parameter of a given rough surface and we have analyzed the roughness of the samples. All the surfaces show nearly Gaussian and unimodal probability density function (pdf) profile roughness with different skewness (γ) and kurtosis (κ) as shown in Figure 2. Almost perfect Gaussian is observed for grit size 800 with $\gamma \approx 0$ and $\kappa \approx 3$. It can be observed that at this roughness, we got maximum equilibrium contact angle or Young's contact angle (θ_c) as observed in Figure 5. The pdfs in Figure 2 have physical significance indicating the Gaussian like profiles are results of PDMS surface roughness being not systematic but random rough surface. For certain cases like grit size 800, the randomness is very close to the Gaussian pdf as revealed from the skewness and kurtosis measures. Depending on the grit size, the static contact angle or Young's contact angle at t = 0 are almost constant with a small uncertainty of ±5°. However, as time evolves, the dynamic contact angles across multiple experiments start to diverge gradually depending on the size of the droplet. We also show the variance of the random roughness of the surface $z(x)$ which was extracted from the confocal image as another input in the robust polynomial regression model. We have calculated the surface roughness based on multiple segments of the confocal image and used it in the regression model as shown in Figure 4. We have carried out multiple (5-10) runs of the same experiments as shown in Figure 5-Figure 6 that generates the data for the statistical modelling. The variations in the experiments are due to various size of the droplets getting introduced in the model which is associated with the variance of the residuals in the later sections.

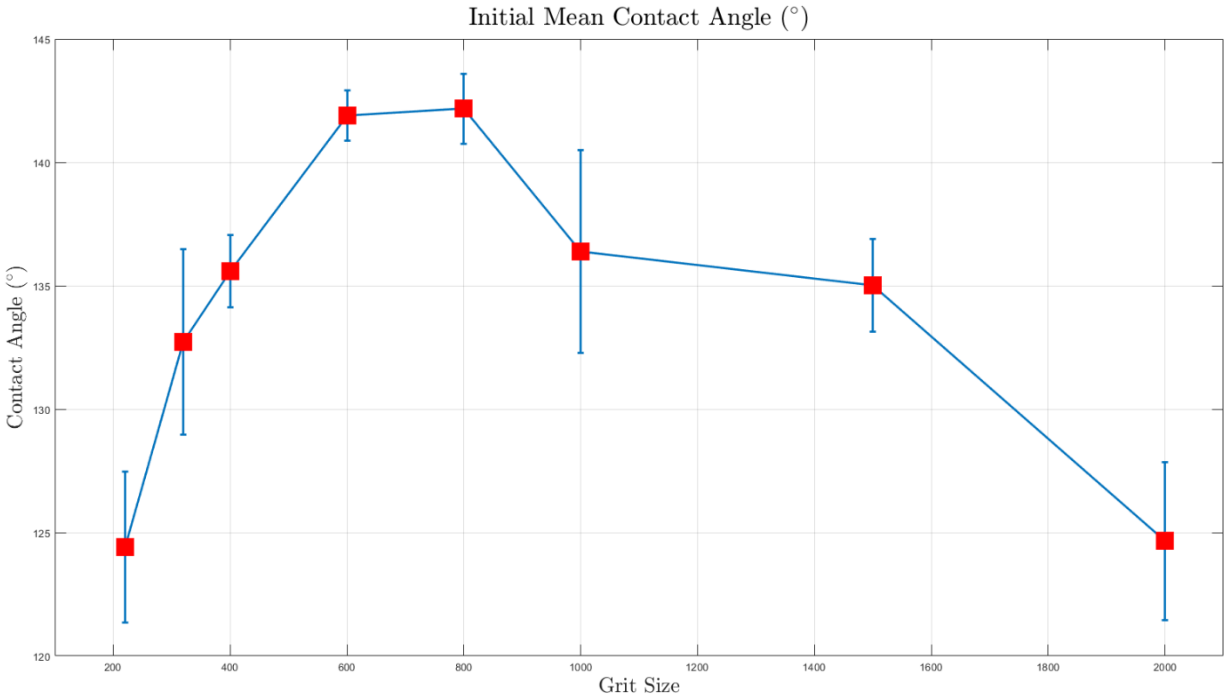

Figure 5: Change in initial mean equilibrium contact angle vs. grit size along with the error bars showing one standard deviation variation between repeated experiments.

Figure 5 shows change in the initial mean equilibrium contact angle at the beginning of the droplet drying experiment. We calculate the mean and one standard deviation error bars for each grit size which shows even for slightly different size of the droplets, the error bars are relatively smaller showing the repeatability of the experiments that was used in the statistical modeling. Figure 5 also shows that the mean contact angles are closely similar and small for the grit sizes of 220 and 2000 whereas it is large for the grit sizes of 800 and 600. Similar to the mean contact angle, rest of the initial droplet properties i.e.

base diameter (in mm), height (in mm), surface (mm^2), volume (mm^3), left contact angle (º) and right contact angle (º) were also shown along with the respective error bars in Figure 6. From our experimental study, we found that the base diameter is the lowest for grit size 600 and both the height and surface are highest whereas the volume of the droplets are fairly similar in size. Figure 6 also shows that the left and right contact angles are very similar indicating nearly symmetric droplet deposition on the random surfaces.

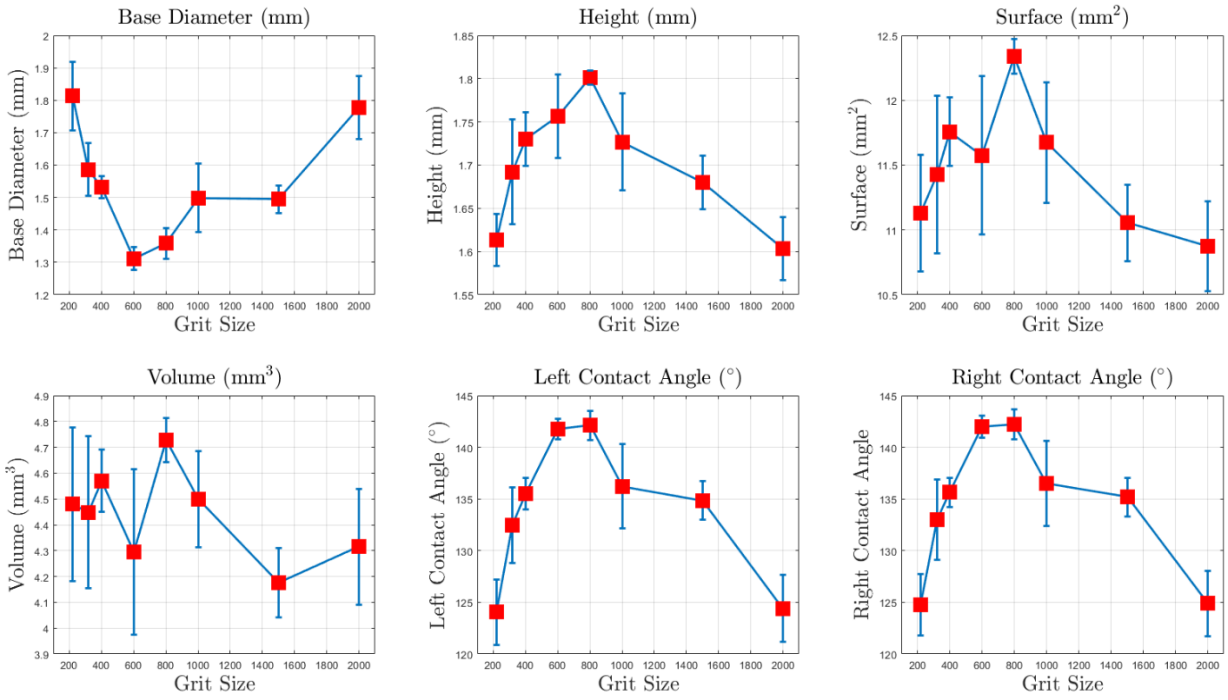

Figure 6: Change in 6 different initial droplet parameters vs. grit size along with the error bars showing one standard deviation variation between repeated experiments.

4. Results for Wetting Behavior

Following the initial values at the beginning of the droplet drying experiments, the temporal evolution of equilibrium contact angle (CA), base diameter (BD), height (*H*), surface periphery (*S*) and volume (*V*) change of drops were then observed. Accordingly, the triple phase contact line (TPCL) and contact angle start to modify.

4.1 Description of the Experimental Dataset

The temporal evolution of wetting behaviors of de-ionized water on structured PDMS surfaces, made with sandpapers of grit sizes 220, 320, 400, 600, 800, 1000, 1500 and 2000 are observed in Figure 7. The variations of BD and CA of drops are clearly observed in these 8 different substrates. For the grit sizes 220 and 2000, instability and larger fluctuations at the last stage of drying are distinguishably noticed in BD and CA curves. It is noted that the base diameters (BD) of the drops show a sudden jump immediately after deposition on coarse substrates, for the grit sizes, 220, 320 and 400 respectively. It clearly shows that the drops did not remain pinned on the substrates during drying. All the wetting characteristic parameters changes with time in a nonlinear fashion. For all the grit sizes in Figure 7, the surface and volume reduce almost linearly with time, while other parameters show strong nonlinear characteristics. In Figure 7, we show multiple experiments for each grit size and the outcome of repeated trials or experiments under the same setting to develop the statistical models using regression methods.

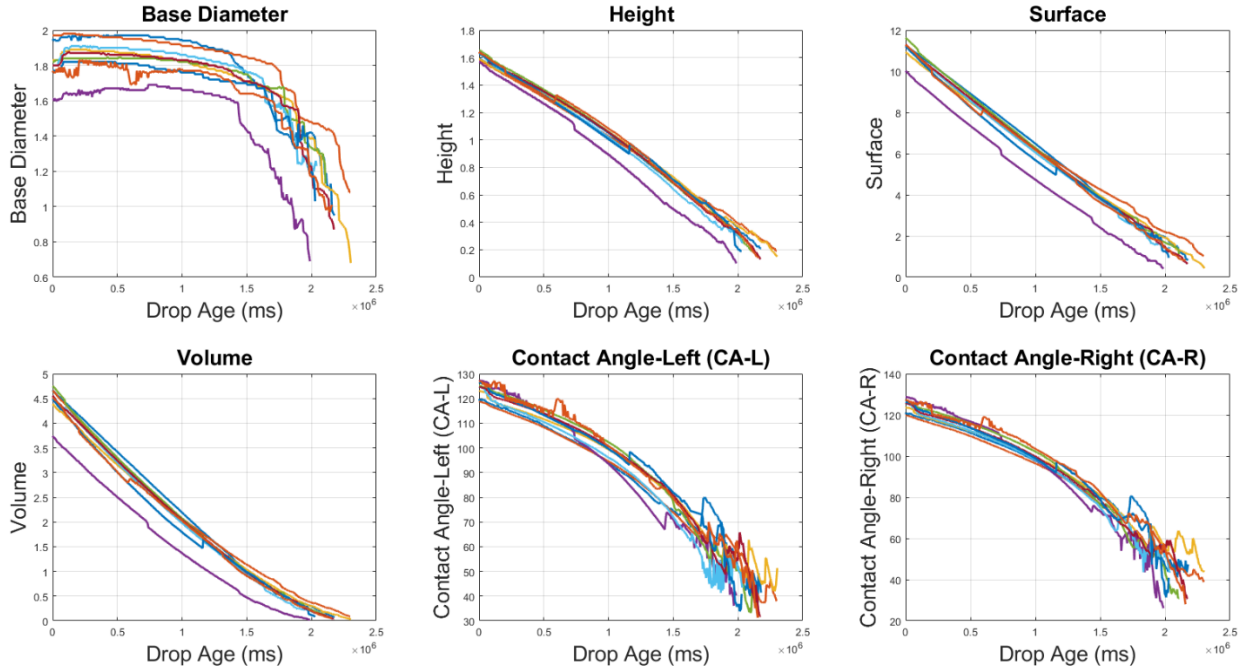
Base Diameter
Base Diameter
Drop Age (ms)
Height
Height
Drop Age (ms)
Surface
Surface
Drop Age (ms)
Volume
Volume
Drop Age (ms)
Contact Angle-Left (CA-L)
Contact Angle-Left (CA-L)
Drop Age (ms)
Contact Angle-Right (CA-R)
Contact Angle-Right (CA-R)
Drop Age (ms)

(a)

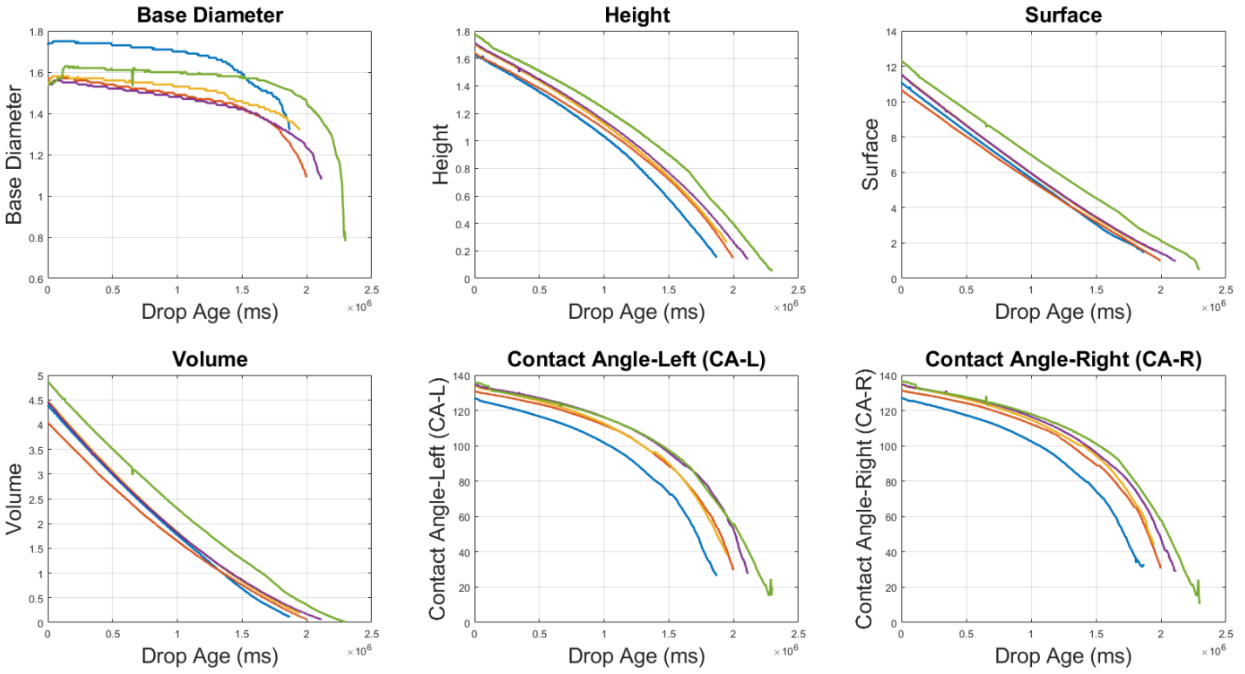
Base Diameter
Base Diameter
Drop Age (ms)
Height
Height
Drop Age (ms)
Surface
Surface
Drop Age (ms)
Volume
Volume
Drop Age (ms)
Contact Angle-Left (CA-L)
Contact Angle-Left (CA-L)
Drop Age (ms)
Contact Angle-Right (CA-R)
Contact Angle-Right (CA-R)
Drop Age (ms)

(b)

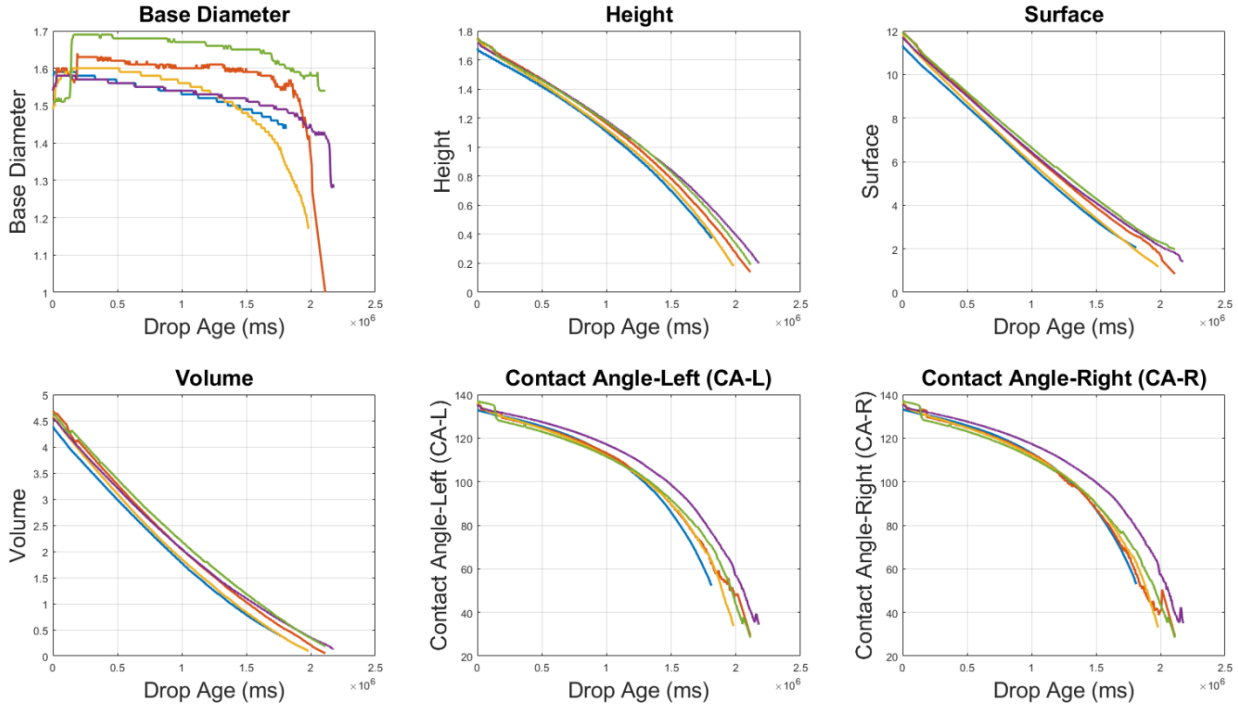
Base Diameter
Base Diameter
Drop Age (ms)
Height
Height
Drop Age (ms)
Surface
Surface
Drop Age (ms)
Volume
Volume
Drop Age (ms)
Contact Angle-Left (CA-L)
Contact Angle-Left (CA-L)
Drop Age (ms)
Contact Angle-Right (CA-R)
Contact Angle-Right (CA-R)
Drop Age (ms)

(c)

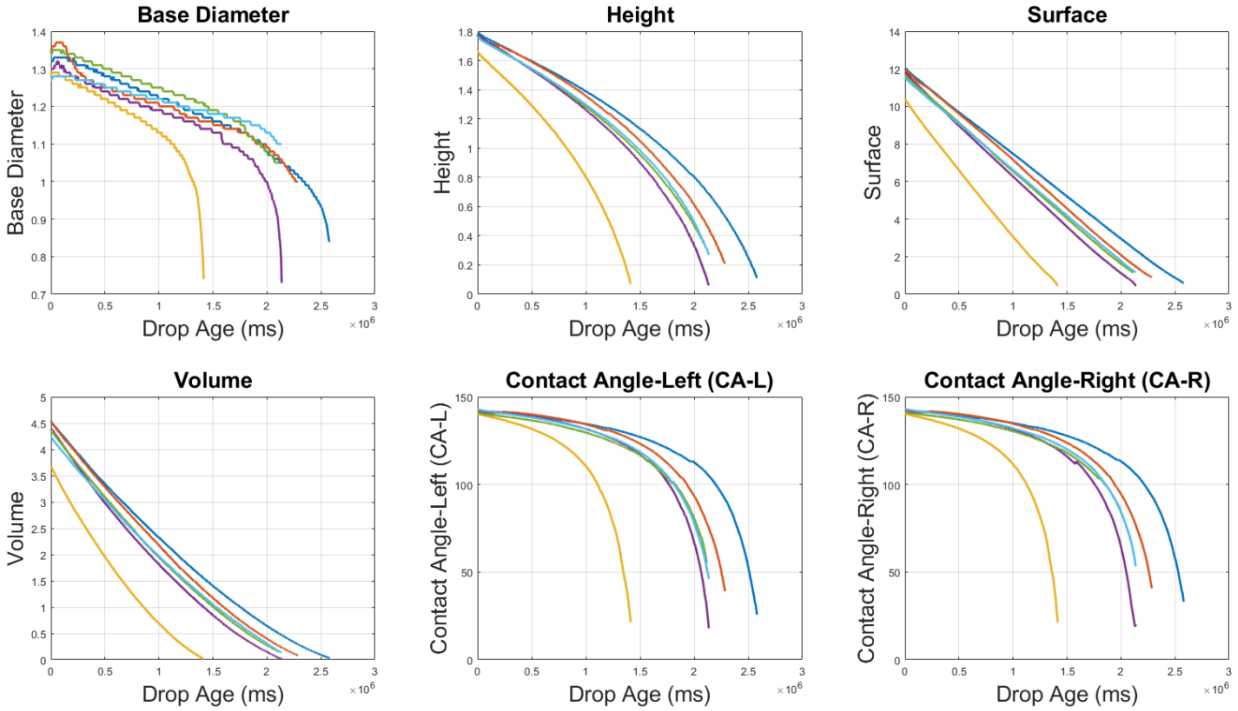
Base Diameter
Base Diameter
Drop Age (ms)
Height
Height
Drop Age (ms)
Surface
Surface
Drop Age (ms)
Volume
Volume
Drop Age (ms)
Contact Angle-Left (CA-L)
Contact Angle-Left (CA-L)
Drop Age (ms)
Contact Angle-Right (CA-R)
Contact Angle-Right (CA-R)
Drop Age (ms)

(d)

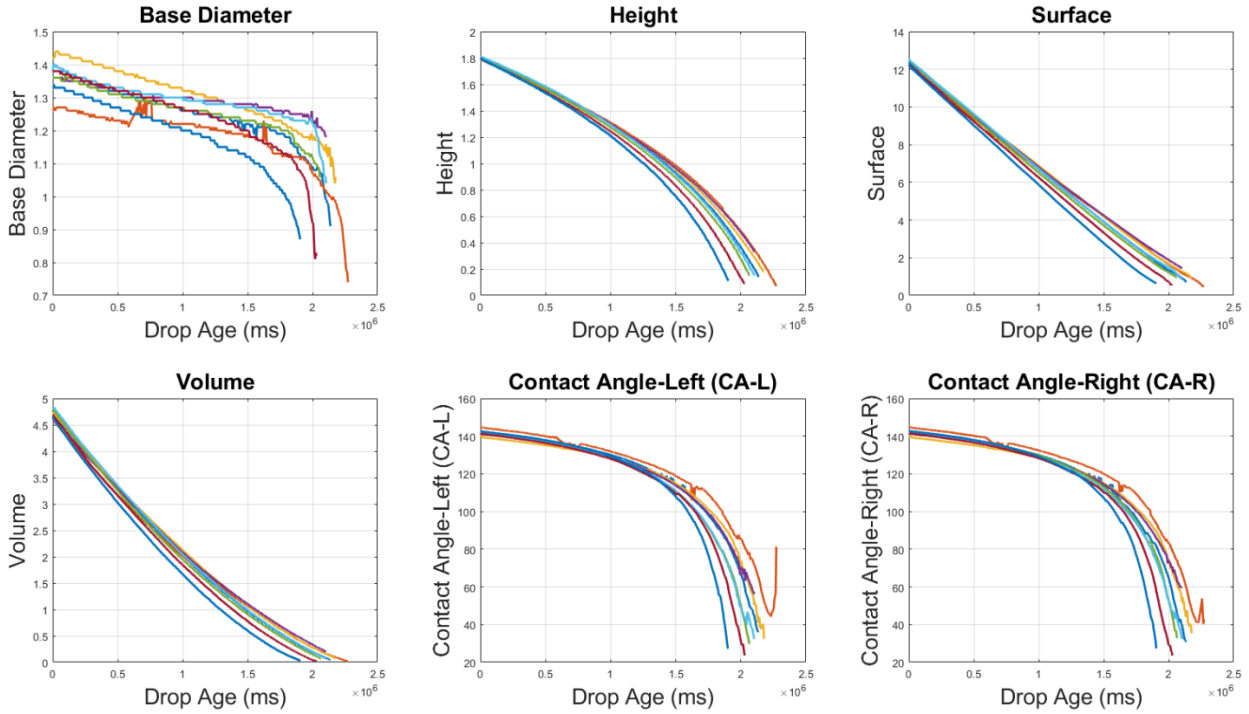
Base Diameter
Base Diameter
Drop Age (ms)
Height
Height
Drop Age (ms)
Surface
Surface
Drop Age (ms)
Volume
Volume
Drop Age (ms)
Contact Angle-Left (CA-L)
Contact Angle-Left (CA-L)
Drop Age (ms)
Contact Angle-Right (CA-R)
Contact Angle-Right (CA-R)
Drop Age (ms)

(e)

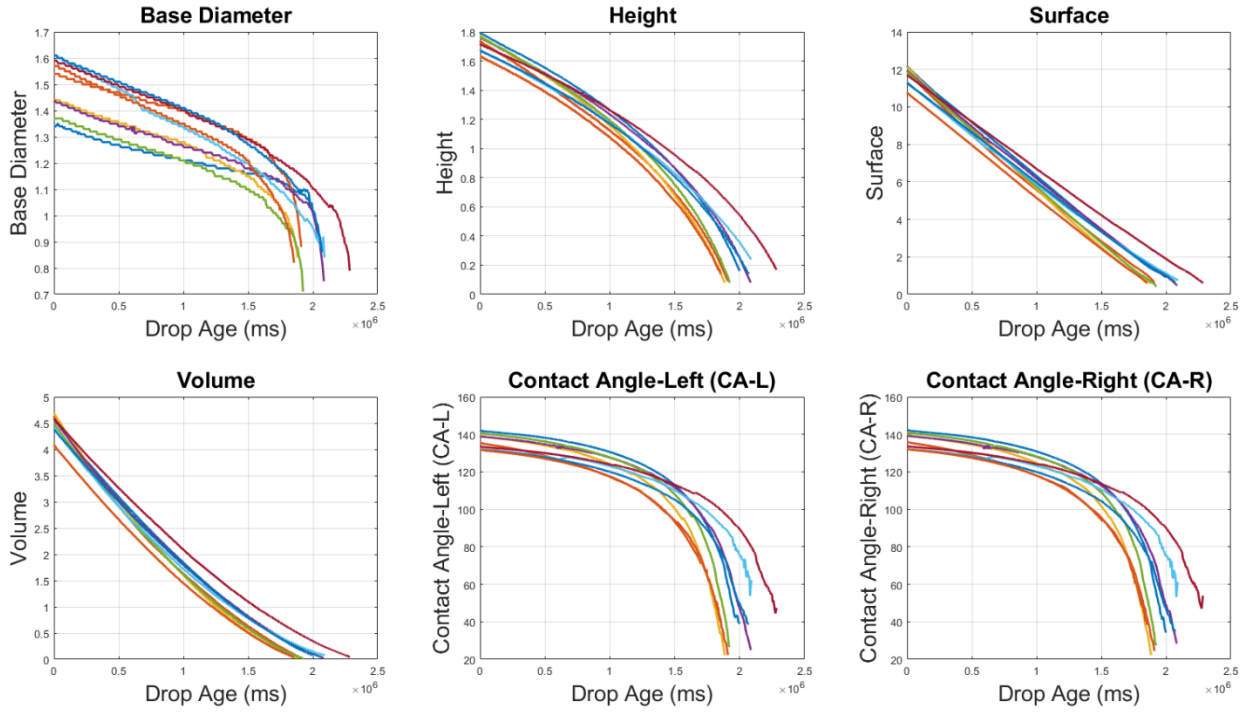
Base Diameter
Base Diameter
Drop Age (ms)
Height
Height
Drop Age (ms)
Surface
Surface
Drop Age (ms)
Volume
Volume
Drop Age (ms)
Contact Angle-Left (CA-L)
Contact Angle-Left (CA-L)
Drop Age (ms)
Contact Angle-Right (CA-R)
Contact Angle-Right (CA-R)
Drop Age (ms)

(f)

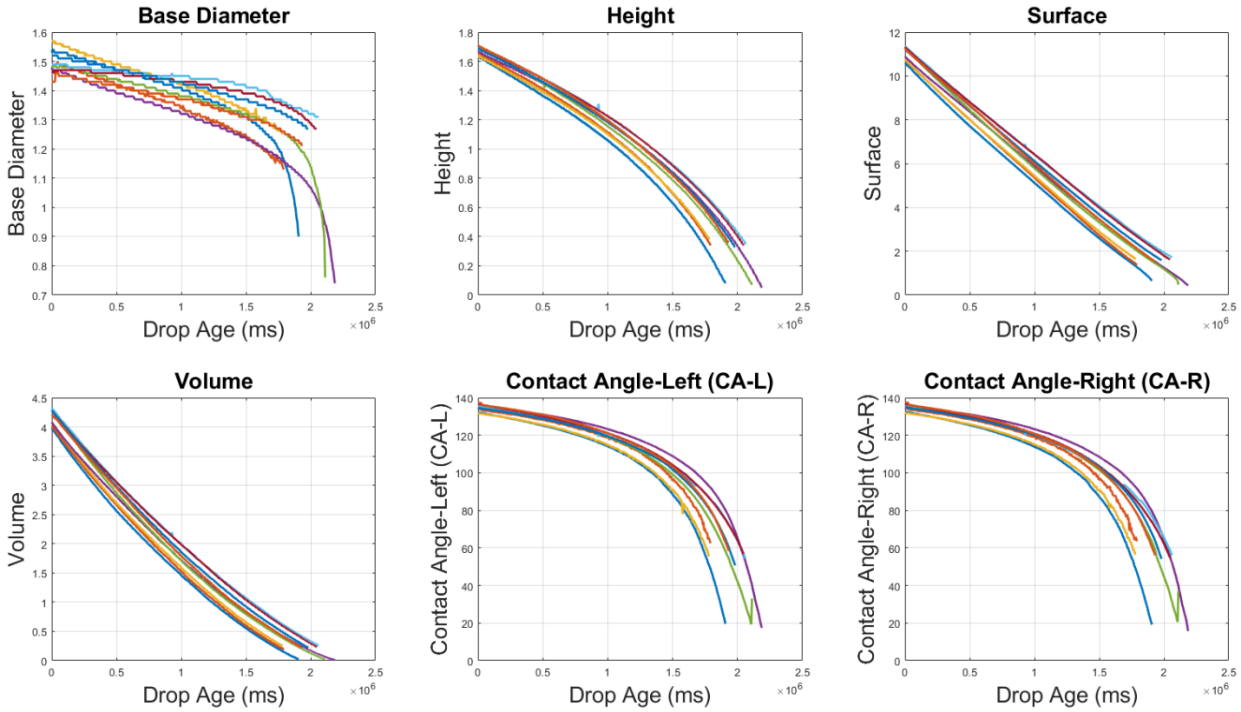

(g)

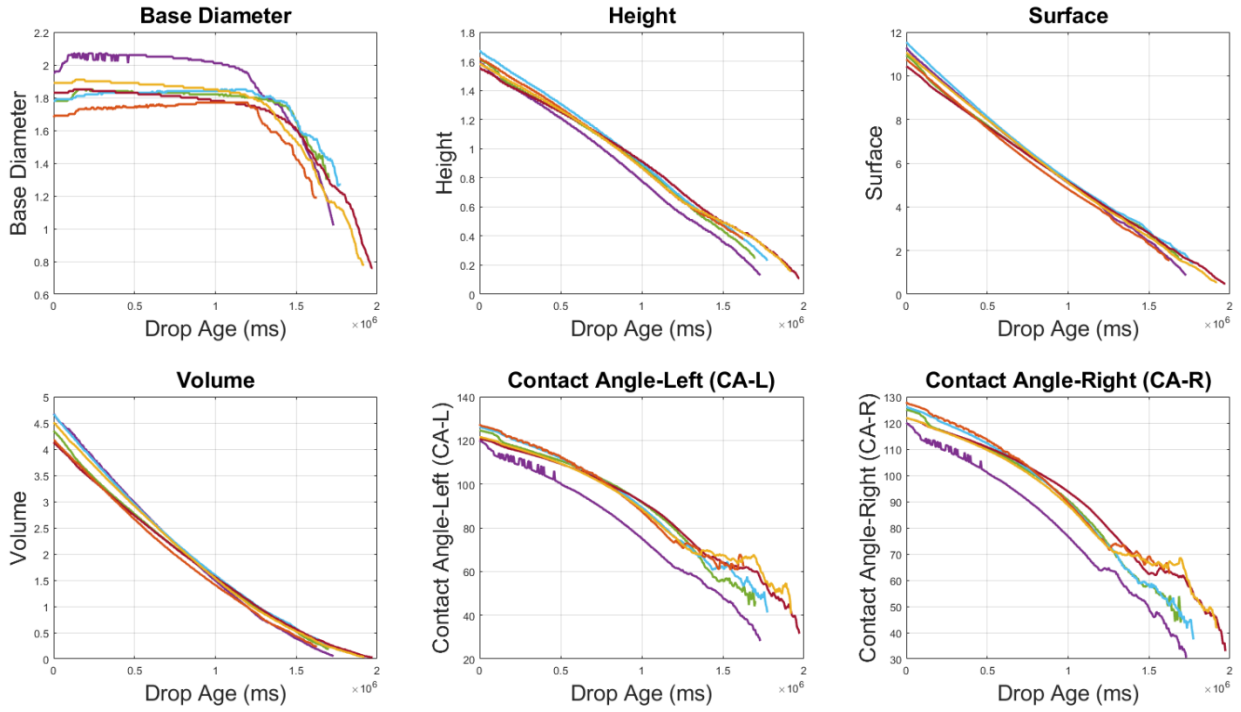

(h)

Figure 7: Temporal evolution of the droplet properties viz. base diameter (mm), height (mm), surface (mm^2), volume (mm^3), contact angle (^{o}), with different surface roughness (a) 220, (b) 320, (c) 400, (d) 600, (e) 800, (f) 1000, (g) 1500, (h) 2000.

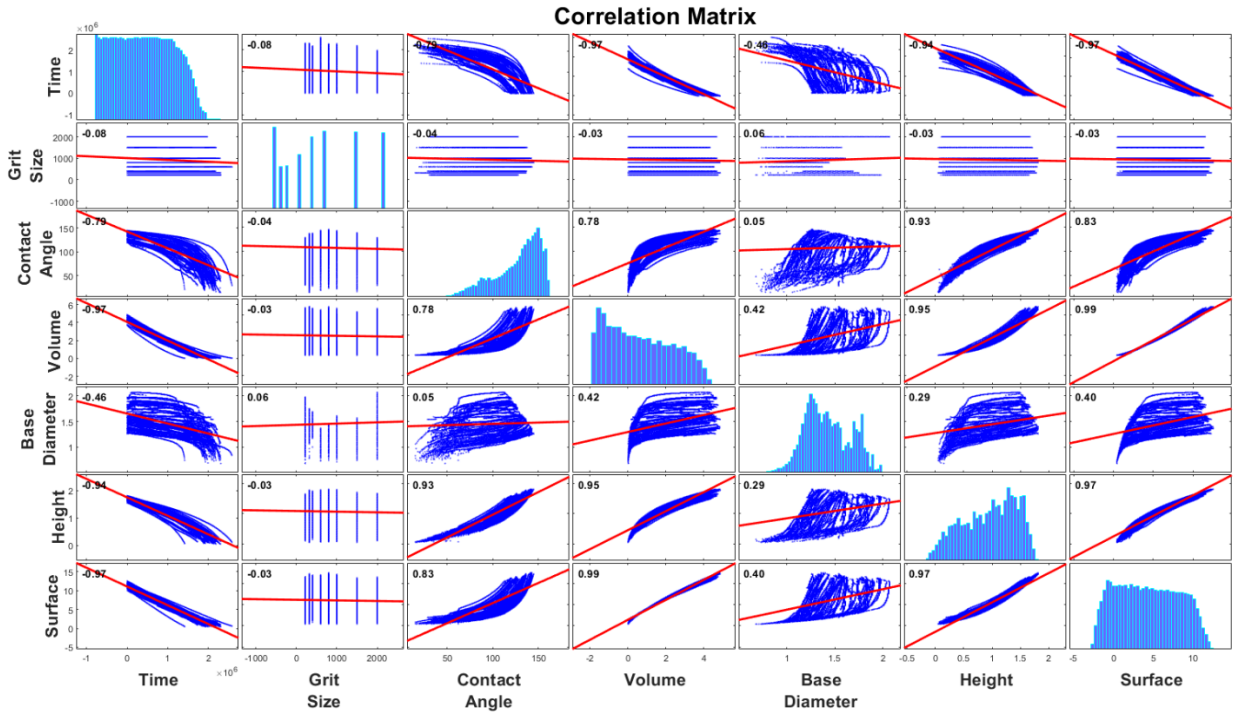

Figure 8: Multivariate correlation matrix plot amongst all the droplet/surface parameters along with the Pearson correlation coefficients (r) for each pair of variables considering all the grit sizes together. Height vs. surface, volume vs. height and surface are found to have high positive correlation i.e. $r \geq 0.95$. Also, volume and surface negatively correlate with time i.e. $r \leq -0.95$, indicating they decrease gradually with time. The principal diagonals indicate the univariate marginal distribution of the dataset and the upper and lower triangular parts indicate bivariate distribution of each variable pairs as scatter plots along with a fitted linear regression plot to show any linear correlation structures in the dataset pairs.

From Figure 7 the contact angles at the right side and left side of droplets are found to be almost symmetric and confirms that there is no inclination of the substrates in any direction. In the data processing stage, all drop evaporation characteristics were carefully screened to identify outliers showing too small droplet size or BD showing sudden large increase, which could have been an indication of the base not remaining fixed or effect of vibration during recording. Such datasets were discarded in the statistical modelling, in the next subsections.

Grit size of the substrates is an independent parameter, all other wetting characteristics change according to that. High correlation between height, surface and volume indicates that the droplet is considered as a part of a spherical cap. The correlation matrix plot in Figure 8 also confirms the nonlinearity between CA vs BD. Low correlation between BD vs CA implies that there are other factors involved, without which we will not be able to quantify and model these two parameters.

4.2 Dependent Parameters and Independent Parameters of the Droplet Drying Experiment

Next, we show that CA vs BD (Figure 9), CA vs H (Figure 10) and CA vs S (Figure 11) vary in highly nonlinear fashion because all of them depend on the roughness of substrates. For coarse grains, like 220, 320 the CA vs BD curves show similar pattern, and it is quite different than the substrates with grit sizes 600, 800, 1000 and 1500. Surface with grit size 400 shows intermediate wetting behavior. Please note that grit size 2000 again shows some similarity like 220, as also found in the earlier sections. Smaller grit size means the number of sharp objects in per unit inch are very low and the object size is big. For a small drop on this kind of surface is more like pure PDMS substrate. On contrary, larger grit

size implies the number of sharp objects is very small and that also leads to smoother PDMS substrates. In the modelling, contact angle, grit size and time were considered to be the independent variables to predict rest of the dependent variables using a robust polynomial regression model.

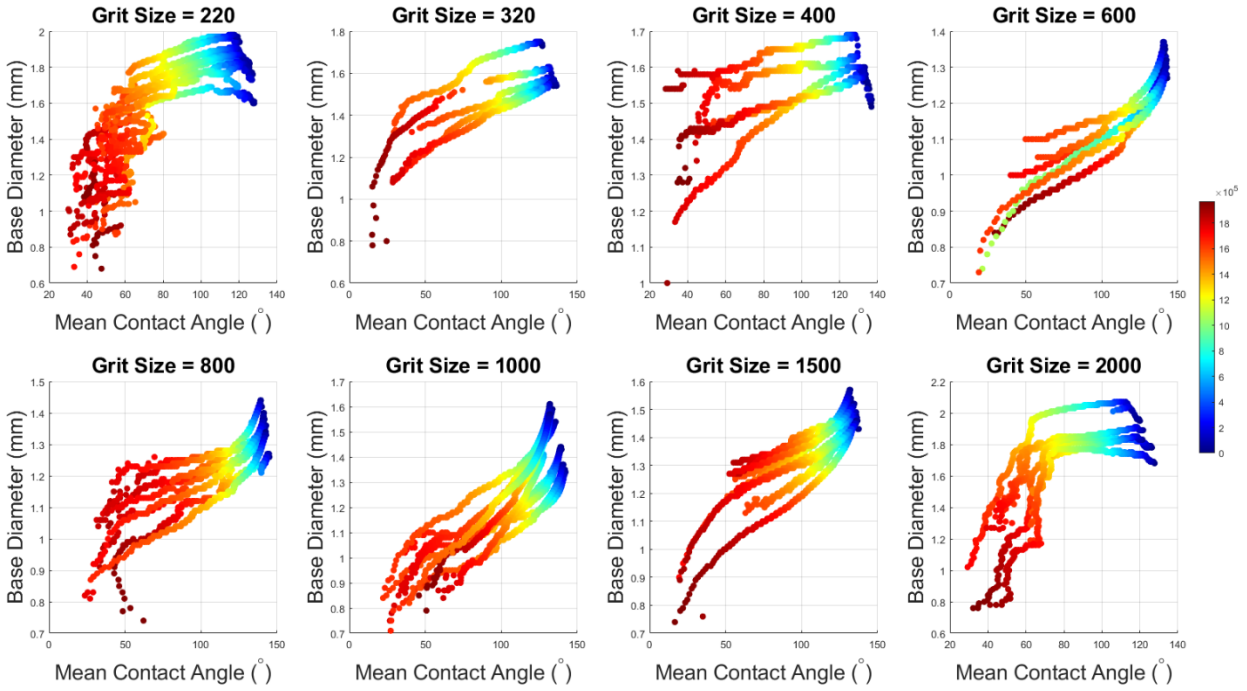

Figure 9: Scatter plots of base diameter vs mean contact angle. The color represents the age of the droplet in ms. Low CA region the trajectories get diverged and as their spread increase.

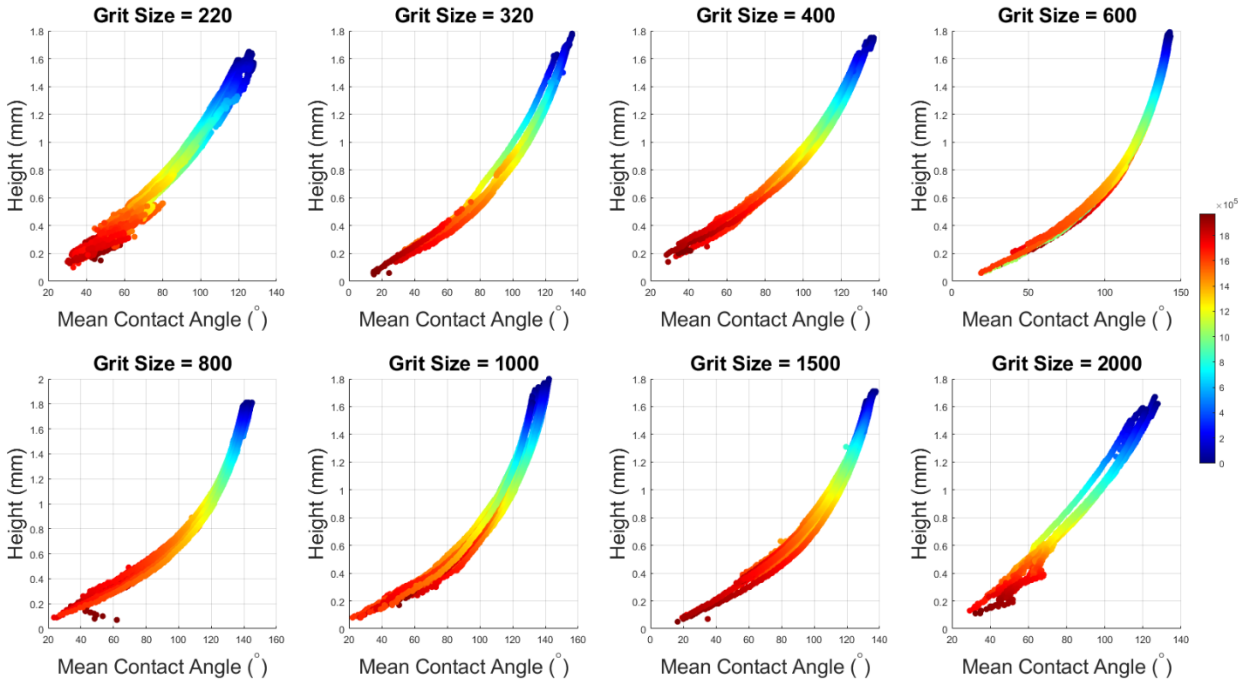

Figure 10: Scatter plots of height vs mean contact angle. The color represents the age of the droplet in ms. Height vs MCA shows slightly nonlinear relationship for grit size = 600-1000.

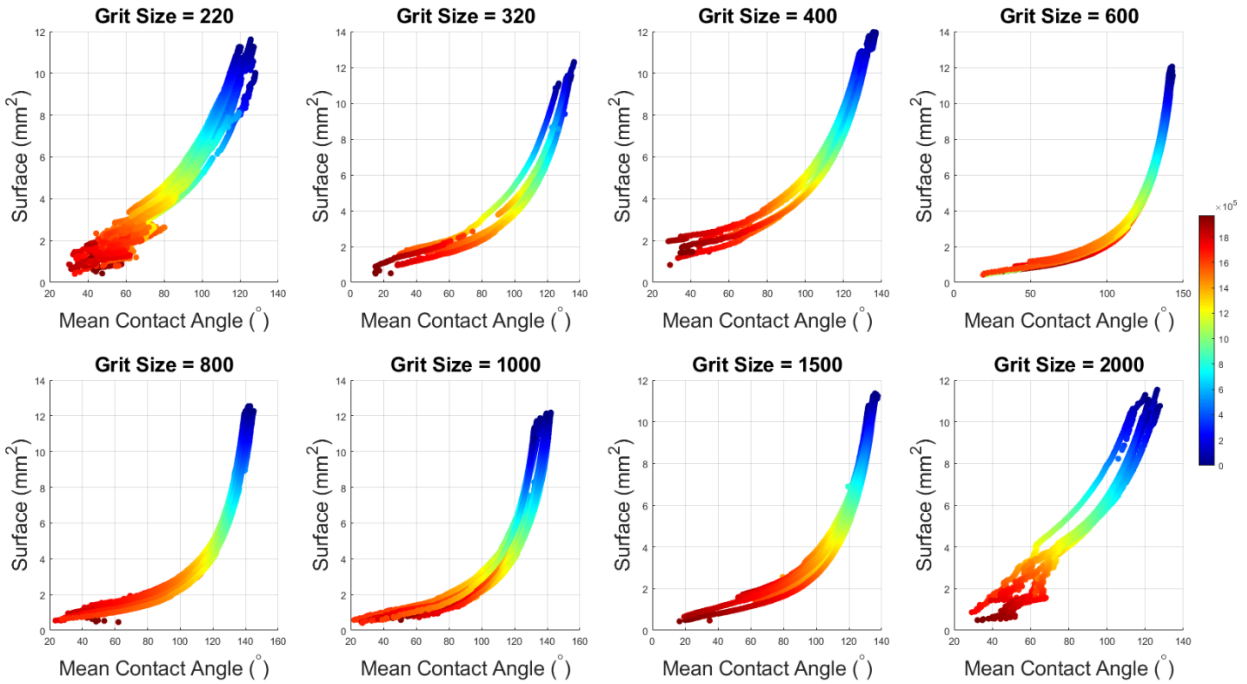

Figure 11: Scatter plots of surface vs mean contact angle. The color represents the age of the droplet in ms. *S* vs. MCA shows stronger nonlinear pattern for wider range of grit size = 320 to 1500.

4.3 Polynomial Regression Modeling of BD as a function of contact angle, grit size and time

Next, we aim to fit a regression model to see how well the three explanatory variables – CA (x_1), grit size (x_2), time (x_3=*t*) can predict the target variable base diameter (y=BD). We use a robust polynomial regression with Andrews weight function since it better prevents overfitting of the regression models in other recent works e.g. [47] while using 5 different polynomial kernels – linear (without interactions), linear with interactions, pure quadratic (without interactions), quadratic with interactions and cubic with interactions as:

$$
\begin{aligned}
y_{\text{linear}} &= \beta_0 + \beta_1 x_1 + \beta_2 x_2 + \beta_3 x_3 + \varepsilon, \quad \varepsilon \sim \mathcal{N}\left(0, \sigma^2\right), \\
y_{\text{interaction}} &= \beta_0 + \beta_1 x_1 + \beta_2 x_2 + \beta_3 x_3 + \beta_4 x_1 x_2 + \beta_5 x_1 x_3 + \beta_6 x_2 x_3 + \beta_7 x_1 x_2 x_3 + \varepsilon, \\
y_{\text{pure-quadratic}} &= \beta_0 + \beta_1 x_1 + \beta_2 x_2 + \beta_3 x_3 + \beta_4 x_1^2 + \beta_5 x_2^2 + \beta_6 x_3^2 + \varepsilon, \\
y_{\text{quadratic}} &= \beta_0 + \beta_1 x_1 + \beta_2 x_2 + \beta_3 x_3 + \beta_4 x_1 x_2 + \beta_5 x_1 x_3 + \beta_6 x_2 x_3 + \beta_7 x_1 x_2 x_3 + \beta_8 x_1^2 + \beta_9 x_2^2 + \beta_{10} x_3^2 + \varepsilon.
\end{aligned}
\tag{1}
$$

In equation (1), the number of terms and the model complexity increases with higher orders of the polynomials where the coefficients $\beta_i, i \in \mathbb{Z}_+$ are estimated in the polynomial regression model where the residuals are usually considered to be zero mean white Gaussian noise with variance σ^2. Although the robustness option (Andrew's criteria) helps to safeguard against overfitting to some extent, a higher order polynomial is likely not to capture the generic pattern in the data showed in Figure 12. This is evident from Figure 13 where the adjusted coefficient of variation (R^2) is found to be highest (R^2=0.8333) for the linear interaction regression model and the predictive accuracy reduces with either decreasing (indicating under-fitting) and increasing model complexity (indicating overfitting) as expected [48]. In the regression modeling the three variables - time, CA and BD are considered as continuous variables. However, as shown in Figure 12, the grit size is sparse and discontinuous in nature due to limited number of experiments that can be possible to carry out. In the regression modeling shown in Figure 13, the distributions of the residuals are also close to univariate normal.

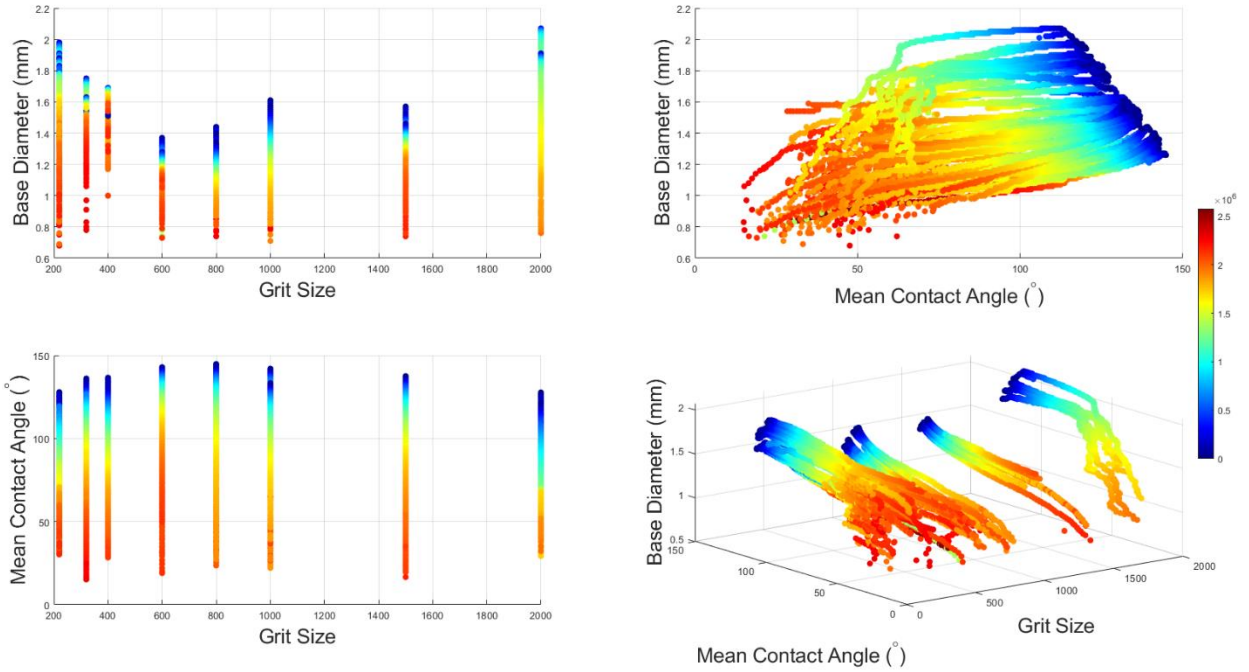

Figure 12: Change of droplet base diameter (BD) as a function of mean contact angle (MCA) and grit size. Scatter plots between the variables are shown and the data-points are colored using the age of the droplet. The BD vs MCA have a smoother variation as compared to other variables.

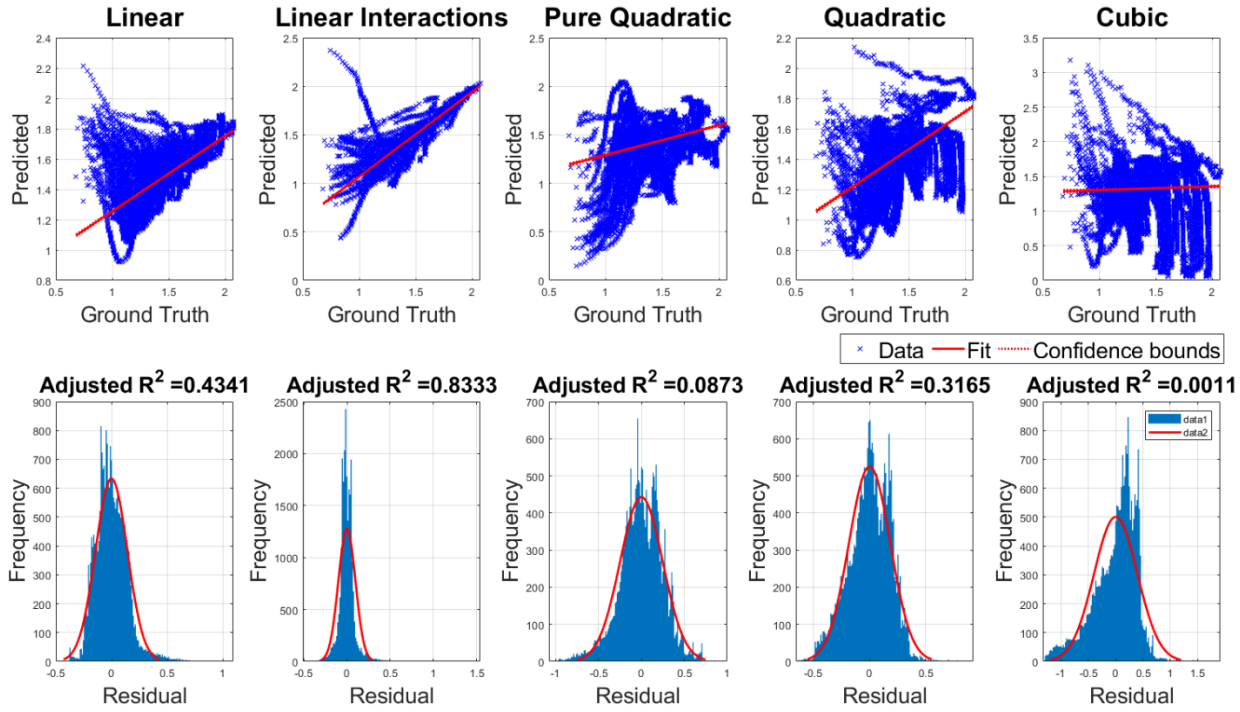

Figure 13: (top panels) Linear, linear interaction, pure quadratic, quadratic, and cubic polynomial regression results to predict BD as a function of time, MCA and grit size. (bottom panels) A univariate Gaussian pdf fitting has been done on the histogram of residuals along with calculating the R^2 values for different orders of the robust polynomial regression models.

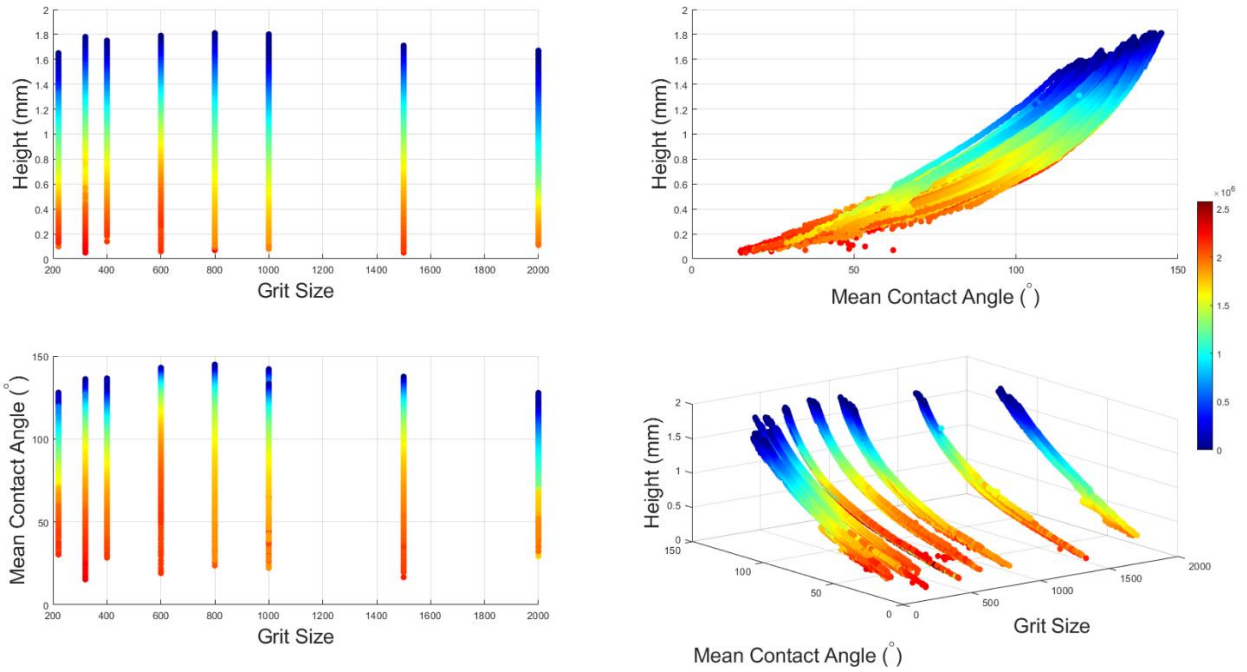

Figure 14: Change of droplet height (*H*) as a function of mean contact angle (MCA) and grit size. Scatter plots between the variables are shown and the data-points are colored using the age of the droplet. The *H* vs MCA have a smoother variation as compared to other variables.

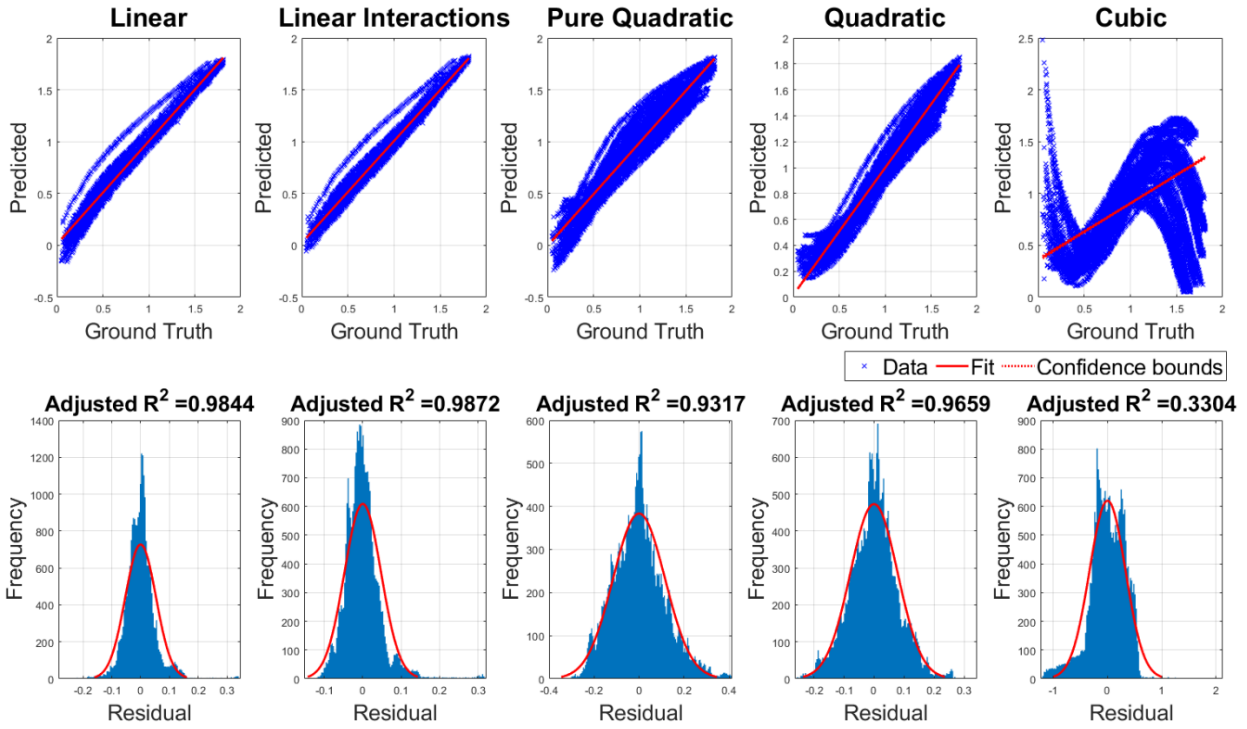

Figure 15: (top panels) Linear, linear interaction, pure quadratic, quadratic, and cubic polynomial regression results to predict *H* as a function of time, MCA and grit size. (bottom panels) A univariate Gaussian pdf fitting has been done on the histogram of residuals along with calculating the R^2 values for different orders of the robust polynomial regression models.

4.4 Polynomial Regression Modeling of Height (H) as a function of contact angle, grit size and time

A similar statistical modeling has been attempted for predicting height as a function of time, grit size and CA as shown in Figure 14 where again the linear interaction model showed highest predictive accuracy (R^2=0.9872) which sharply falls with more complex models in the robust polynomial regression framework. Histogram fits to the residuals show close to Gaussian distribution in Figure 15.

4.5 Polynomial Regression Modeling of Surface (S) as a function of contact angle, grit size and time

Similar to the prediction of BD and height, the problem of predicting surface area (S) can also be attempted for all grit sizes using the data showed in Figure 16. It is evident that for all the above robust polynomial regression models, the linear interaction model still yields the highest predictive accuracy (R^2=0.9736) indicating simple yet meaningful interpretation of such compact models for predicting BD, H, S as nonlinear interacting functions of time, CA, and grit size. The histogram fittings of residuals follow similar univariate Gaussian nature as before. As a summary for all three statistical modeling tasks the linear interaction models shows the best performance in terms of the adjusted R^2 value. Prediction of S and H show high accuracy with adjusted R^2 ranging between 0.97-0.98, as compared to the BD.

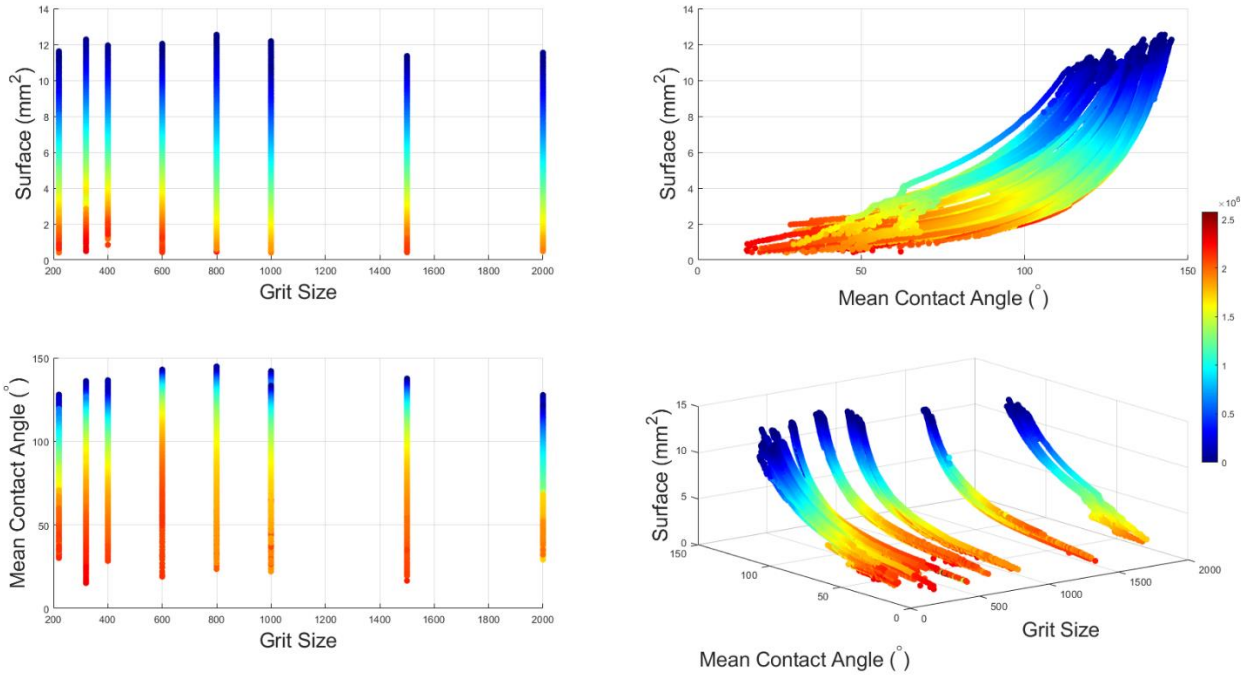

Figure 16: Change of droplet surface (S) as a function of mean contact angle (MCA) and grit size. Scatter plots between the variables are shown and the data-points are colored using the age of the droplet. The S vs MCA have a smoother variation as compared to other variables.

From the above modeling results was aimed to find out the relationships between the drop drying parameters and to quantify it with the surface structures. Now if we look at the most accurate predictions of the BD, height, and surface area of the droplets, it is found that the most reliable model is the linear interaction model for all grit sizes for all parameters. But height and surface, showed better fitting than BD. The BD is directly associated with the drop adsorption or liquid substrate interaction. Moreover, the time-evolution of BD is more complicated than height or surface evolution because of the water-trapping phenomenon. Normality of the residuals in most of the accurate models also indicate that the patterns in the multivariate droplet drying data has been successfully captured in the statistical models while the residuals do not contain any crucial information to be captured by the model.

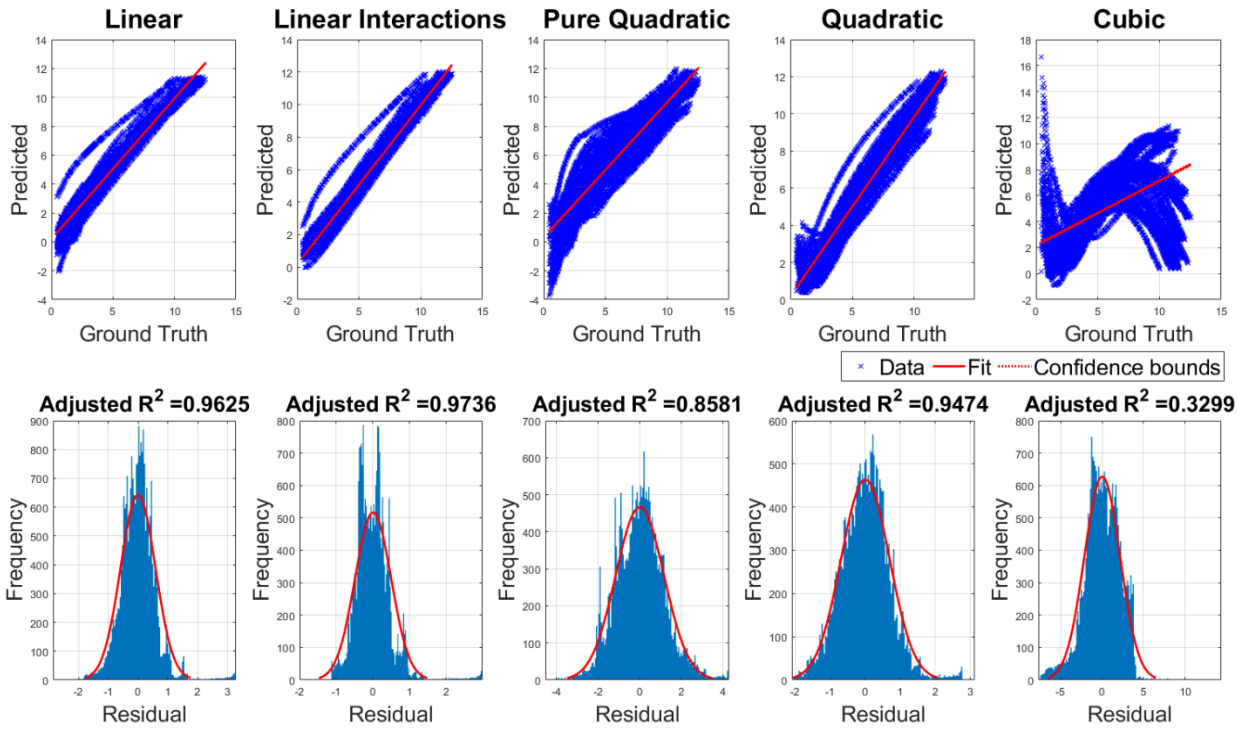

Figure 17: (top panels) Linear, linear interaction, pure quadratic, quadratic, and cubic polynomial regression results to predict S as a function of time, MCA and grit size. (bottom panels) A univariate Gaussian pdf fitting has been done on the histogram of residuals along with calculating the R^2 values for different orders of the robust polynomial regression models.

5. Conclusions

This paper advances the current knowledge of droplet wetting characteristics during evaporation, especially on structured random surfaces of hydrophobic nature. Amongst the methodological advances, firstly the random roughnesses on PDMS by sandpaper introduce hydrophobic nature in the PDMS substrate without adding any new material on the substrate. This is cost effective and quite easy to build. Secondly, for a particular grit-size, the surface roughness reaches its optimum position with maximum contact angle. For the grit sizes 220 and 2000, the prominent fluctuations observed in CA measurements, which emphasize the mode changing of droplets from wetting to dewetting. The above-mentioned roughness also showed uniqueness in their wetting patterns. Extreme two points of random porosity showed proper similarity in their base-diameter and CA measurements. They showed maximum wetting property and minimum contact angle in comparison with ordinary PDMS surface. Normally PDMS shows partial hydrophobicity and high Contact angle hysteresis because of its polymeric heterogeneity. The roughness changes the hydrophobicity of the surface naturally. But the adhesive nature of the polar water molecules to the surface shows nearly similar kind of nature, except for higher porous randomness introduced by 220 grits of sandpaper to the surface and 2000 grits of roughness. This implies that water molecules could be trapped inside the pores for 220 grits. That is why we got the fluctuations in those volume vs. drop-age plots and BD vs. grit size plots. The dewetting dynamics is faster for 2000 grits, though it shows smaller CA than others, therefore, the dewetting property is modified because of its closely packed randomness. Thirdly, the strong nonlinearity between the base diameter, surface and height with contact angle leads to linear interaction equations to fit for all the grit sizes as a function of time to capture their temporal evolution. The main contribution of this paper is to develop a robust statistical model of the wetting characteristics on surface of different roughness. There are many experimental studies on this topic but there are very few works which has attempted to model the

relationship between the involved parameters since such processes are very complex to model using the first principle or analytical methods.

In the future, similar experimental investigations and statistical modelling can be carried out on other complex soft matters on different surface characteristics with increasing roughness, especially in the context of biological and medical applications, perhaps involving infectious diseases. In such application specific domains, analytical expressions are difficult to derive as an extension of simple spherical cap modelling. This is because it needs a lot of assumptions for governing physics modeling like smooth and horizontally placed surface with deionized water which may further vary with the adhesive properties of the liquid. This justifies our generalized statistical modeling approach is transferable in other complex surface-liquid interaction scenarios as well. The aim of this paper is not to explain the mechanism how the evaporation happens on complex surfaces, rather identifying the most important variables and establishing an empirical or statistical model of wetting characteristics between the wetting parameters during droplet drying as the evaporation happens. In future works, we shall aim to explain the mechanics of the evaporation on rough surfaces.

Acknowledgement

MDC thanks SERB, India for providing national post-doctoral fellowship (PDF/2016/001151/PMS) to carry out the research. SD was partially supported by the ERDF Deep Digital Cornwall project number: 05R18P02820.

Authorship contribution statement

MDC – Conceptualization, Methodology, Investigation, Writing - Original Draft, Funding acquisition; **SD** – Software, Validation, Formal analysis, Data Curation, Writing - Review & Editing, Visualization, **AGB** – Resources, Supervision, Project administration, Methodology, Investigation; **AK** – Investigation, Methodology.

Data Availability Statements

The data that support the findings of this study are available from the corresponding author upon reasonable request.

References

[1] M. de A. M. M. Ferraz, J. B. Nagashima, B. Venzac, S. Le Gac, and N. Songsasen, "3D printed mold leachates in PDMS microfluidic devices," *Scientific Reports*, vol. 10, no. 1, pp. 1–9, 2020.
[2] T. Fujii, "PDMS-based microfluidic devices for biomedical applications," *Microelectronic Engineering*, vol. 61, pp. 907–914, 2002.
[3] R. Mukherjee, R. C. Pangule, A. Sharma, and I. Banerjee, "Contact instability of thin elastic films on patterned substrates," *The Journal of Chemical Physics*, vol. 127, no. 6, p. 064703, 2007.
[4] M. Srinivasarao, "Nano-optics in the biological world: beetles, butterflies, birds, and moths," *Chemical reviews*, vol. 99, no. 7, pp. 1935–1962, 1999.
[5] P. Vukusic and J. R. Sambles, "Photonic structures in biology," *Nature*, vol. 424, no. 6950, pp. 852–855, 2003.
[6] J. Sun and B. Bhushan, "Nanomanufacturing of bioinspired surfaces," *Tribology International*, vol. 129, pp. 67–74, 2019.
[7] A. Giacomello, M. Chinappi, S. Meloni, and C. M. Casciola, "Metastable wetting on superhydrophobic surfaces: Continuum and atomistic views of the Cassie-Baxter-Wenzel transition," *Physical Review Letters*, vol. 109, no. 22, p. 226102, 2012.

[8] M. Azadi Tabar, F. Barzegar, M. H. Ghazanfari, and M. Mohammadi, "On the applicability range of Cassie-Baxter and Wenzel equation: a numerical study," *Journal of the Brazilian Society of Mechanical Sciences and Engineering*, vol. 41, no. 10, pp. 1–12, 2019.
[9] S. Ghaffari, M. Aliofkhazraei, G. B. Darband, A. Zakeri, and E. Ahmadi, "Review of superoleophobic surfaces: Evaluation, fabrication methods, and industrial applications," *Surfaces and Interfaces*, vol. 17, p. 100340, 2019.
[10] C. Li, J. Zhang, J. Han, and B. Yao, "A numerical solution to the effects of surface roughness on water-coal contact angle," *Scientific Reports*, vol. 11, no. 1, pp. 1–12, 2021.
[11] K. Birdi, *Self-assembly monolayer structures of lipids and macromolecules at interfaces*. Springer Science & Business Media, 2006.
[12] M. Berczeli and Z. Weltsch, "Enhanced wetting and adhesive properties by atmospheric pressure plasma surface treatment methods and investigation processes on the influencing parameters on HIPS polymer," *Polymers*, vol. 13, no. 6, p. 901, 2021.
[13] Q. Lin, C. Wang, K. Xie, L. Wang, and R. Sui, "Comparative study on wetting of smooth and rough silica surface by molten Sn-3.5 Ag-2Ti alloys," *Ceramics International*, vol. 47, no. 20, pp. 29205–29212, 2021.
[14] H. Bagheri, M. Aliofkhazraei, M. Gheytani, H. Masiha, A. S. Rouhaghdam, and T. Shahrabi, "Growth and internal microstructure of micro-arc oxidized MgO-based nanocomposite coating," *Surface and Coatings Technology*, vol. 283, pp. 1–9, 2015.
[15] R. Bhardwaj and A. Agrawal, "How coronavirus survives for days on surfaces," *Physics of Fluids*, vol. 32, no. 11, p. 111706, 2020.
[16] S. Kumar, "Insight on the evaporation dynamics in reducing the COVID-19 infection triggered by respiratory droplets," *Physics of Fluids*, vol. 33, no. 7, p. 072004, 2021.
[17] S. Sarkar, T. Roy, A. Roy, S. Moitra, R. Ganguly, and C. M. Megaridis, "Revisiting the supplementary relationship of dynamic contact angles measured by sessile-droplet and captive-bubble methods: Role of surface roughness," *Journal of Colloid and Interface Science*, vol. 581, pp. 690–697, 2021.
[18] S. Chatterjee, J. S. Murallidharan, A. Agrawal, and R. Bhardwaj, "Designing antiviral surfaces to suppress the spread of COVID-19," *Physics of Fluids*, vol. 33, no. 5, p. 052101, 2021.
[19] N. Hutasoit, B. Kennedy, S. Hamilton, A. Luttick, R. A. R. Rashid, and S. Palanisamy, "Sars-CoV-2 (COVID-19) inactivation capability of copper-coated touch surface fabricated by cold-spray technology," *Manufacturing Letters*, vol. 25, pp. 93–97, 2020.
[20] M. Nosonovsky and B. Bhushan, *Multiscale dissipative mechanisms and hierarchical surfaces: friction, superhydrophobicity, and biomimetics*. Springer Science & Business Media, 2008.
[21] D. E. Packham, "Surface energy, surface topography and adhesion," *International Journal of Adhesion and Adhesives*, vol. 23, no. 6, pp. 437–448, 2003.
[22] P. Goel, M. Dutta Choudhury, A. B. Aqeel, X. Li, L.-H. Shao, and H. Duan, "Effect of Thermal Conductivity on Enhanced Evaporation of Water Droplets from Heated Graphene-PDMS Composite Surfaces," *Langmuir*, vol. 35, no. 21, pp. 6916–6921, 2019.
[23] S. Hong, R. Wang, X. Huang, and H. Liu, "Facile one-step fabrication of PHC/PDMS anti-icing coatings with mechanical properties and good durability," *Progress in Organic Coatings*, vol. 135, pp. 263–269, 2019.
[24] C. Yang, F. Wang, W. Li, J. Ou, C. Li, and A. Amirfazli, "Anti-icing properties of superhydrophobic ZnO/PDMS composite coating," *Applied Physics A*, vol. 122, no. 1, p. 1, 2016.
[25] P. G. Gezer, S. Brodsky, A. Hsiao, G. L. Liu, and J. L. Kokini, "Modification of the hydrophilic/hydrophobic characteristic of zein film surfaces by contact with oxygen plasma treated PDMS and oleic acid content," *Colloids and Surfaces B: Biointerfaces*, vol. 135, pp. 433–440, 2015.
[26] A. Putra, A. Kakugo, H. Furukawa, J. P. Gong, Y. Osada, T. Uemura, and M. Yamamoto, "Production of bacterial cellulose with well oriented fibril on PDMS substrate," *Polymer Journal*, vol. 40, no. 2, pp. 137–142, 2008.

[27] Y. Liu, H. Gu, Y. Jia, J. Liu, H. Zhang, R. Wang, B. Zhang, H. Zhang, and Q. Zhang, "Design and preparation of biomimetic polydimethylsiloxane (PDMS) films with superhydrophobic, self-healing and drag reduction properties via replication of shark skin and SI-ATRP," *Chemical Engineering Journal*, vol. 356, pp. 318–328, 2019.
[28] M. S. U. Rasel and J.-Y. Park, "A sandpaper assisted micro-structured polydimethylsiloxane fabrication for human skin based triboelectric energy harvesting application," *Applied Energy*, vol. 206, pp. 150–158, 2017.
[29] X.-W. Zhang, G.-Z. Li, G.-G. Wang, J.-L. Tian, Y.-L. Liu, D.-M. Ye, Z. Liu, H.-Y. Zhang, and J.-C. Han, "High-performance triboelectric nanogenerator with double-surface shape-complementary microstructures prepared by using simple sandpaper templates," *ACS Sustainable Chemistry & Engineering*, vol. 6, no. 2, pp. 2283–2291, 2018.
[30] D. Kim, H. M. Lee, and Y.-K. Choi, "Large-sized sandpaper coated with solution-processed aluminum for a triboelectric nanogenerator with reliable durability," *RSC Advances*, vol. 7, no. 1, pp. 137–144, 2017.
[31] Y. He, C. Jiang, X. Cao, J. Chen, W. Tian, and W. Yuan, "Reducing ice adhesion by hierarchical micro-nano-pillars," *Applied Surface Science*, vol. 305, pp. 589–595, 2014.
[32] S. Baba, K. Sawada, K. Tanaka, and A. Okamoto, "Dropwise Condensation on a Hierarchical Nanopillar Structured Surface," *Langmuir*, vol. 36, no. 34, pp. 10033–10042, 2020.
[33] H. Ogihara, J. Xie, J. Okagaki, and T. Saji, "Simple method for preparing superhydrophobic paper: spray-deposited hydrophobic silica nanoparticle coatings exhibit high water-repellency and transparency," *Langmuir*, vol. 28, no. 10, pp. 4605–4608, 2012.
[34] A. Kuzminova, A. Shelemin, O. Kylián, M. Petr, J. Kratochvil, P. Solar, and H. Biederman, "From super-hydrophilic to super-hydrophobic surfaces using plasma polymerization combined with gas aggregation source of nanoparticles," *Vacuum*, vol. 110, pp. 58–61, 2014.
[35] J. Bravo, L. Zhai, Z. Wu, R. E. Cohen, and M. F. Rubner, "Transparent superhydrophobic films based on silica nanoparticles," *Langmuir*, vol. 23, no. 13, pp. 7293–7298, 2007.
[36] J. Drelich, "Guidelines to measurements of reproducible contact angles using a sessile-drop technique," *Surface innovations*, vol. 1, no. 4, pp. 248–254, 2013.
[37] D. Kwok, T. Gietzelt, K. Grundke, H.-J. Jacobasch, and A. W. Neumann, "Contact angle measurements and contact angle interpretation. 1. Contact angle measurements by axisymmetric drop shape analysis and a goniometer sessile drop technique," *Langmuir*, vol. 13, no. 10, pp. 2880–2894, 1997.
[38] J. A. Rogers and R. G. Nuzzo, "Recent progress in soft lithography," *Materials Today*, vol. 8, no. 2, pp. 50–56, 2005.
[39] G. Brenn, "Concentration fields in evaporating droplets," *International Journal of Heat and Mass Transfer*, vol. 48, no. 2, pp. 395–402, 2005.
[40] H. Hu and R. G. Larson, "Analysis of the effects of Marangoni stresses on the microflow in an evaporating sessile droplet," *Langmuir*, vol. 21, no. 9, pp. 3972–3980, 2005.
[41] J. M. Stauber, S. K. Wilson, B. R. Duffy, and K. Sefiane, "Evaporation of droplets on strongly hydrophobic substrates," *Langmuir*, vol. 31, no. 12, pp. 3653–3660, 2015.
[42] D. Tam, V. von ARNIM, G. McKinley, and A. Hosoi, "Marangoni convection in droplets on superhydrophobic surfaces," *Journal of Fluid Mechanics*, vol. 624, pp. 101–123, 2009.
[43] B. Bhushan and S. Chilamakuri, "Non-Gaussian surface roughness distribution of magnetic media for minimum friction/stiction," *Journal of Applied Physics*, vol. 79, no. 8, pp. 5794–5796, 1996.
[44] J. Liu, E. Lu, H. Yi, M. Wang, and P. Ao, "A new surface roughness measurement method based on a color distribution statistical matrix," *Measurement*, vol. 103, pp. 165–178, 2017.
[45] "3D Optical Surface Metrology System Leica DCM 3D." [Online]. Available: https://www.leica-microsystems.com/products/light-microscopes/p/leica-dcm-3d/
[46] "OCA – Software." [Online]. Available: https://www.dataphysics-instruments.com/products/oca/software/

[47] S. Das, X. Chen, M. P. Hobson, S. Phadke, B. van Beest, J. Goudswaard, and D. Hohl, "Surrogate regression modelling for fast seismogram generation and detection of microseismic events in heterogeneous velocity models," *Geophysical Journal International*, vol. 215, no. 2, pp. 1257–1290, 2018.
[48] S. Rogers and M. Girolami, *A first course in machine learning*. CRC Press, 2015.